https://doi.org/10.5194/acp-2020-845
Preprint. Discussion started: 13 October 2020

Atmospheric Chemistry and Physics Discussions

Potential impact of aerosols on convective clouds revealed by Himawari-8 observations over different terrain types in eastern China

Tianmeng Chen[a,b,c], Zhanqing Li[b,*], Ralph A. Kahn[b,d], Chuanfeng Zhao[a,*], Daniel Rosenfeld[e], Jianping Guo[c], Wenchao Han[a,b], Dandan Chen[c]

a. State Key Laboratory of Remote Sensing Sciences, and College of Global Change and Earth System Science, Beijing Normal University, Beijing, 100875, China

b. Department of Atmospheric and Oceanic Sciences & Earth System Science Interdisciplinary Center, University of Maryland, College Park, Maryland 20740, USA

c. State Key Laboratory of Severe Weather, Chinese Academy of Meteorological Sciences, Beijing 100081, China

d. Earth Sciences Division, NASA Goddard Space Flight Center, Greenbelt, Maryland 20771 USA

e. Institute of Earth Sciences, Hebrew University, Jerusalem, Israel

* To whom all correspondence should be addressed

Zhanqing Li

Email: zli@atmos.umd.edu

Chuanfeng Zhao

Email: czhao@bnu.edu.cn

https://doi.org/10.5194/acp-2020-845
Preprint. Discussion started: 13 October 2020

Atmospheric Chemistry and Physics Discussions

Abstract

Convective clouds are common and play a major role in Earth's water cycle and energy balance; they may even develop into storms and cause severe rainfall events. To understand the convective cloud development process, this study investigates the impact of aerosols on convective clouds by considering the influence of both topography and diurnal variation of radiation. By combining texture analysis, clustering and thresholding methods, we identify all convective clouds in two warm seasons (May-September, 2016-2017) in eastern China based on Himawari-8 Level 1 data. Having a large diurnally resolved cloud data together with surface meteorological and environmental measurements, we investigate convective cloud properties and their variation, stratified by elevation and diurnal change. We then analyze the potential impact of aerosol on convective clouds under different meteorological conditions and topographies. In general, convective clouds tend to occur preferentially under polluted conditions in the morning, which reverses in the afternoon. Convective cloud fraction first increase then decrease with aerosol loading, which may contribute to this phenomenon. Topography and diurnal meteorological variations may affect the strength of aerosol microphysical and radiative effects. Updraft is always stronger along the windward slopes of mountains and plateaus, especially in northern China. The prevailing southerly wind near the foothills of mountains and plateaus is likely to contribute to this windward strengthening of updraft and to bring more pollutant into the mountains, thereby strengthening the microphysical effect, invigorating convective clouds. By comparison, over plain, aerosol decreases surface heating and suppresses convection by blocking solar radiation reaching the surface.

Key Words

Himawari-8; convective cloud; aerosol-cloud interactions, topographic effects on cloud

https://doi.org/10.5194/acp-2020-845
Preprint. Discussion started: 13 October 2020

Atmospheric Chemistry and Physics Discussions

1. Introduction

Convective cloud is important for Earth's energy balance and the water cycle. Changes in the distribution or triggering time of convective cloud can have a large impact on the climate system (Stocker et al., 2013). Previous studies have shown that aerosol particles in the atmosphere can affect the formation and development of convective clouds, through both radiative and microphysical effects (Ramanathan et al., 2001; Tao et al., 2012; Altaratz et al., 2014; Rosenfeld et al., 2014a, 2014b; Li et al., 2016; Zhao et al., 2018a; Yang et al., 2019), which can dramatically affect the weather and climate(Zhao et al., 2020).

Aerosol particles generally cool the surface by scattering the downward solar radiation (McCormick and Ludwig, 1967; Charlson et al., 1992), whereas light-absorbing aerosol can additionally warm the atmosphere above the surface (Ackerman et al., 2000). These aerosol radiative effects change the surface radiation budget and the atmospheric temperature profile directly, thereby altering the onset time of convective cloud formation and precipitation (Feingold et al., 2005; Wang et al., 2013; Zhou et al., 2020).

Aerosols, by acting as cloud condensation nuclei (CCN) and/or ice nuclei (IN), can also affect the formation and growth of cloud droplets (Rosenfeld, 2000; Kaufman et al., 2002; Garrett et al., 2004; Lohmann and Feichter, 2005; Zhao et al., 2012), which is regarded as the aerosol microphysical effect. For constant cloud liquid water content, increases in aerosol particle number concentration can produce more but smaller cloud droplets, thus increasing cloud albedo (Twomey and Warner, 1967; Twomey, 1974). This effect, called the "Twomey effect", is a well-established influence on cloud properties in polluted environments (Kaufman and Nakajima, 1993; Feingold et al., 2003). Smaller cloud droplets can increase cloud lifetime and reduce precipitation (Albrecht, 1989), whereas for some deep convective cloud, the latent heat released by the formation of more and smaller ice particles can invigorate deep convection and

https://doi.org/10.5194/acp-2020-845
Preprint. Discussion started: 13 October 2020

increase rain rate (Andreae et al., 2004; Kaufman et al., 2005; Rosenfeld et al., 2008; Li et al., 2011; Fan et al., 2013; Li et al., 2019). For cases of thin clouds, smaller cloud droplets enhance cloud thermal emissivity, trap more longwave radiation within the atmosphere and alter cloud development (Garrett and Zhao, 2006; Zhao and Garrett, 2015).

Many previous studies show that the interactions between aerosols and weather variables are complex (Stevens and Feingold, 2009; Altaratz et al., 2014), making it challenging to untangle aerosol effects from meteorological factors that influence convective clouds. As different types of clouds form under different meteorological conditions, some previous observational studies attempted to classify clouds into different types, to distinguish aerosol effects in various meteorological regimes (Andreae et al., 2004; Khain et al., 2005; Li et al., 2011; Gryspeerdt and Stier, 2012; Gryspeerdt et al., 2014; Qiu et al., 2017). Other studies consider different cloud types as different stages of convective development, to identify aerosol effects on convective cloud evolution, stratified by meteorological conditions (Chen et al., 2016; Guo et al., 2018).

Meteorological conditions can change during the day and can vary from one place to another. For example, convective cloud and precipitation maxima tend to occur in the early morning over open ocean, but in the late afternoon or early evening over land, driven primarily by temporal differences in the radiative forcing (Chang et al., 1995; Garreaud and Wallace, 1997; Sui et al., 1997; Zhou et al., 2008; Li et al., 2010). Other studies show that the impact of terrain on the convective cloud can also be complex (Roe, 2005; Houze Jr., 2012), and that the meteorological factors that control convection can be affected by terrain (Romatschke and Houze Jr., 2010, 2011a, b). Diurnal variation of solar radiation can alter wind circulation in a valley, and therefore may control the spatial distribution of convective cloud in mountainous regions (Kirshbaum and Durran, 2004, 2005; Kirshbaum et al., 2007; Romatschke et al., 2010).

https://doi.org/10.5194/acp-2020-845
Preprint. Discussion started: 13 October 2020

In recent years, studies also attempted to explore the effects of topography on aerosol-precipitation interactions. Lynn et al. (2007) simulated the aerosol effect on orographic precipitation using the WRF model and found that the intensity of orographic precipitation is suppressed in more polluted environments. However, when the cold rain process is involved, precipitation is delayed but intensified (Givati and Rosenfeld, 2004; Rosenfeld and Givati, 2006; Xiao et al., 2015; Yang et al., 2016c). When light-absorbing aerosol is present, radiative heating in the atmosphere can produce enhanced instability, which may trigger disastrous precipitation, especially late in the day (Fan et al., 2015). These studies revealed some potential influences of aerosol on orographic precipitation from either model-simulations or from several specific observed cases. Only a few studies include sufficient observational data to analyze the relationships between aerosol and orographic convective cloud statistically. This might be due to a lack of observational data in the past with sufficiently high spatial and temporal resolution.

Although polar orbiting satellites provide high spatial resolution data, they cannot track the diurnal development of convective clouds. In contrast, geostationary satellite data can track the evolution of convective clouds over the entire day at a slightly lower spatial resolution (Chakraborty et al., 2015, 2016). The launch of the Japanese next-generation geostationary satellite Himawari-8 in October 2014 rendered an opportunity to study aerosol effects on convective clouds throughout the day. The diurnal variation in different terrain types may be particularly strong due to amplified variations in radiation and sunshine duration by terrain (Li and Weng, 1987, 1988, 1989). The current study aims to characterize the differences between convective clouds in polluted and clean environments, untangling the probable influence of topography on the way aerosols affect convective clouds, and to explore how the effects of aerosols change diurnally. To achieve this goal, we first develop an automatic method of identifying convective clouds using geostationary satellite data, and then assess how aerosol effects change during the day and in different topographic regions of eastern China.

https://doi.org/10.5194/acp-2020-845
Preprint. Discussion started: 13 October 2020

Atmospheric Chemistry and Physics Discussions

The paper is organized as follows: Section 2 introduces the study region and data selection. The method is described in Section 3. Section 4 presents the temporal and spatial distributions of convective cloud and discusses the possible impact by aerosol on convective cloud over different terrains. In section 5, we give a brief summary.

2. Study region and data

2.1 Region of interest

Rapid economic and industrial growth has brought heavy pollution to China, especially to eastern China, in recent decades. Thus, high aerosol loading over this area provides a natural laboratory for us to study the aerosol impact on convective clouds (Guo et al., 2011). In addition, eastern China has relatively complex topography, where convective clouds can be triggered and develop differently, leading to convective cloud regimes having distinctive diurnal change patterns. We show the terrain distribution and the mean concentration of particles with aerodynamic diameters smaller than 2.5 μm ($PM_{2.5}$) during May-September in 2016-2017 over eastern China in Figure 1. Generally, terrain height (TH) tends to increase from east to west in this region, and $PM_{2.5}$ mass concentration is generally higher over the plains and lower over mountain ranges and plateaus. In order to investigate how these landscapes impact cloud fraction and convective cloud diurnal variation, we chose the area with longitudes from 105°E to 125°E, and latitudes from 20°N to 45°N as the region of interest (ROI) for this study.

2.2 Data

a. Himawari-8 data

The first in a new generation of Japanese geostationary meteorology satellite, named Himawari-8, was launched in 2014. It carries a state-of-art optical sensor, the Advanced Himawari Imager (AHI), which can provide significantly high resolution observations of the Earth system from space (0.5 or 1 km for visible and near-infrared bands at the sub-spacecraft point and 2 km for infrared bands) and time (around 10 min for Full Disk and 2.5 min for sectored regions) from space (Bessho et al., 2016). These advantages

https://doi.org/10.5194/acp-2020-845
Preprint. Discussion started: 13 October 2020

make it possible to detect rapid weather changes, especially the triggering and development of convective cloud. The geostationary sub-spacecraft point is located at 140.7°E over the equator, so most of our ROI is covered.

In this study, we use the Himawari-8 L1 gridded data from the Japan Aerospace Exploration Agency (JAXA) P-Tree system to develop a convective cloud identification method and investigate how aerosols impact convective clouds over eastern China. This dataset is generated by the Earth Observation Research Center (JAXA/EORC) from Himawari Standard Data, with re-sampling to equal latitude-longitude grids. (For more detail, see https://www.eorc.jaxa.jp/ptree/userguide.html ; last accessed: Oct. 2018 .) The channels we use here are centered at 0.64 μm, 11.2 μm, and 12.4 μm, with a spatial resolution of 0.02°×0.02° and a temporal resolution of 10 min.

b. MODIS cloud mask

We use the MODIS/Aqua MYD35 cloud mask data (Wilson et al., 2014) to validate the convective cloud identification method developed here. Cloud mask data at 1 km resolution (from the MYD35 Cloud_Mask product; web address: https://modis.gsfc.nasa.gov/data/dataprod/mod35.php; last accessed: Sep. 2018) is used to compare with the near-simultaneous cloud identification result from our method.

c. Particulate matter (PM) data

In previous studies, aerosol optical depth (AOD) (Andreae, 2009;Niu and Li, 2012;Wang et al., 2018), visibility (Chen et al., 2016), aerosol concentration with diameters between 100 nm and 3 μm (Zhao et al., 2018b;Yang et al., 2019;Zhao et al., 2019), and particulate matter up to 10 μm in diameter (PM_{10}) (Guo et al., 2016) were used as proxies for cloud concentration nuclei (CCN). However, satellite AOD retrievals can only be made in cloud-free conditions, and near-cloud retrievals are frequently influenced by cloud contamination (Li et al., 2009). In addition, remote-sensing methods cannot distinguish the part of the CCN size spectrum smaller than

https://doi.org/10.5194/acp-2020-845
Preprint. Discussion started: 13 October 2020

about 0.05 μm from atmospheric gas molecules. On the other hand, particulate matter can be measured from the surface or aircraft under all-sky conditions. Particle size up to 10 μm may be much larger than the typical scale of CCN, so we consider particle matter up to 1 μm (PM_1) or 2.5 μm ($PM_{2.5}$) in size as a CCN proxy. Due to the limited availability of PM_1 measurement in eastern China, we chose $PM_{2.5}$ as an indicator of different CCN levels in the environment for this study.

Figure 1 also shows the mean value of $PM_{2.5}$ measured at 1205 ground-based stations across eastern China during the warm months (May-September) in 2016-2017. The average $PM_{2.5}$ mass concentration generally lies between 20 and 60 μg/m^3, with higher values over the Beijing-Tianjin-Hebei region. Although not uniformly distributed, the ground stations cover almost all regions in eastern China. Note that these stations provide hourly observations of PM_{10} and $PM_{2.5}$ concentrations.

d. MERRA-2 reanalysis

In order to assess the impact of meteorological factors on convective clouds, and to analyze the dependence of aerosol effects on convective cloud fraction, we adopt meteorological variables from the second Modern-Era Retrospective analysis for Research and Applications (MERRA-2) reanalysis dataset (web address: https://gmao.gsfc.nasa.gov/reanalysis/MERRA-2/; last accessed: Oct. 2019). MERRA-2 is the latest atmospheric reanalysis produced by NASA's Goddard Earth Observing System Data Assimilation System Version 5 (GEOS-5), using a new generation of satellite observation sources from 1979 to the present (Gelaro et al., 2017). In this study, we adopt the temperature at 2 m, relative humidity at 700 hPa and 850 hPa, vertical velocity at 925 hPa and 850 hPa, and surface specific humidity to evaluate how convective cloud fraction changes with respect to terrain height under different meteorological conditions, and to gain insight into whether the aerosol effects are independent of other factors that might influence convective cloud triggering and development during daytime. We obtained all these parameters at a spatial resolution

https://doi.org/10.5194/acp-2020-845
Preprint. Discussion started: 13 October 2020

of 0.5°×0.5°, and a temporal resolution of 3 hours. Based on the findings in previous studies, we chose the following factors to characterize the dynamics and thermodynamics of the environment:

Lower-tropospheric stability (LTS). The lower-tropospheric static stability is defined by Klein and Hartmann (1993) as the inversion strength of the atmosphere. Chen et al. (2016) adopted this LTS definition to distinguish between stable and unstable cloud profiles and to analyze the independence of aerosol effect on clouds. In this study, we use this parameter to assess how the lower atmosphere stability influences the performance of convective clouds. The formula of LTS can be written as

$$LTS = \theta_{700\,hPa} - \theta_{surface} \quad (1)$$

$\theta_{surface}$, which represent the potential temperature at the surface, is calculated from the air temperature at 2 m; the potential temperature at 700 hPa ($\theta_{700\ hPa}$) is directly extracted from MERRA-2 pressure level dataset.

Potential Temperature. Temperature, especially lower-level atmospheric temperature, plays a critical role in triggering the development of convective clouds. As air temperature decreases systematically with altitude in most places, it is not proper to directly compare temperatures over different terrain. As the potential temperature is conserved regardless of height, it reflects the near-surface heating to some extent. Additionally, Wang et al. (2018) point out that selecting potential temperature avoids some duplication of temperature and humidity information. Thus, potential temperature is adopted in this study.

Vertical velocity. Vertical velocities at 850 hPa (ω_{850}) and 925 hPa (ω_{925}) are chosen to investigate the role of vertical airflow in convection. As vertical motion over different terrain may vary, this factor can produce large differences in convective cloud occurrence frequency. We use ω_{850} and ω_{925} to represent the low-level dynamical conditions for terrain above and below 1000 m, respectively. $\omega>0$ represents downward air motion, whereas $\omega<0$ means the air motion is upward. Uncertainty lies in the

https://doi.org/10.5194/acp-2020-845
Preprint. Discussion started: 13 October 2020

different distances between the 850 hPa and 925 hPa level and cloud base. There are likely large differences in the updraft strength between these two levels and the cloud base in some cases. However, in the formation of convective clouds, the vertical velocity between the surface and cloud base is more essential in transporting vapor and energy to higher levels (Lee et al., 2019). As these two levels cover most of the surfaces above and below 1000 m and can reflect the vertical velocities beneath cloud to some extent, we chose to use them as reference values to represent the dynamical conditions when convective clouds occur.

Relative humidity. Water vapor supply is essential to the formation and development of convective clouds (Redelsperger et al., 2002;Chakraborty et al., 2018) and is a crucial component of cloud water condensation and evaporation in aerosol-cloud interactions (Altaratz et al., 2014). As convective cloud formation is more sensitive to the under-cloud and near-surface water vapor content, similar to vertical velocity, relative humidity (RH) data at 700 hPa (RH_{700}, for regions with TH$\geqslant$1000 m), 850 hPa (RH_{850}, for regions with TH<1000 m) and the specific humidity at the surface (q) are employed.

3. Methods

3.1 A convective cloud identification method

Numerous previous studies have attempted to develop methods for detecting and classifying cloud features, including convective clouds, based on satellite observations. One of the most common methods for identifying cloud is thresholding (Williams and Houze Jr., 1987). However, Wielicki and Welch (1986) found that the identified cloud fraction depends strongly on threshold values, as cumulus cloud reflectance varies greatly within individual clouds and at cloud edges. As a result, many studies now adopt digital image processing to help identify shallow convective clouds more accurately.

One widely used image processing method is textural analysis, which adopts second-

https://doi.org/10.5194/acp-2020-845
Preprint. Discussion started: 13 October 2020

Atmospheric Chemistry and Physics Discussions

order statistics representing the texture of the digital image, as first proposed by Haralick (Haralick et al., 1973). This method, known as the gray level co-occurrence matrix (GLCM) method, was applied by Welch et al. (1988a, b) in their LandSat data analysis of marine stratocumulus cloud texture. The GLCM is a matrix of counts/frequencies of grey values for pairs of pixels, whose relative positions are defined by the polar coordinates (d, θ). The formula can be written as:

$$GLCM(i,j,d,\theta) = Pr\{I(x_1,y_1) = i, I(x_2,y_2) = j\}\ x_1,x_2 \in m \text{ and } y_1,y_2 \in n \quad (2)$$

where Pr{E} denotes the probability of event E, I represents the image matrix of size m×n, (x_1,y_1) and (x_2, y_2) are the two elements in I with gray tone value i and j, which are separated by distance d in direction θ. The unit of d is a pixel, and θ always takes 0°, 45°, 90°, and 135°. The maximum difference between i and j defines the size of GLCM. When the frequency of the $(i, j)^{th}$ element is more concentrated near the off-diagonal of the GLCM, the image contains more complex texture. To define texture properties from the GLCM, several image statistical variables are derived from this matrix, including "contrast", "homogeneity", "energy", and "entropy" (Haralick, 1979;Welch et al., 1988b;Baum et al., 1997;Bottino and Ceballos, 2014). The "contrast" measures the intensity contrast between a pixel and its neighbors, assessed over the entire image. "Homogeneity" measures the closeness to the diagonal of the GLCM element distribution. "Energy", also termed the angular second moment, measures the complexity of the image, and "entropy" measures the degree of randomness, evaluated over the entire image. The formulas are:

$$Contrast = \sum_{i,j} |i-j|^2 GLCM(i,j) \quad (3)$$

$$Homogeneity = \sum_{i,j} \frac{GLCM(i,j)}{1+|i-j|} \quad (4)$$

$$Energy = \sum_{i,j} GLCM(i,j)^2 \quad (5)$$

$$Entropy = \sum_{i,j} GLCM(i,j) \ln\,[GLCM(i,j)] \quad (6)$$

https://doi.org/10.5194/acp-2020-845
Preprint. Discussion started: 13 October 2020

The objective of this section is to identify new-born and mature convective clouds. As the edges of convective clouds tend to be very sharp (Purdom, 1976), large differences between i and j can produce large ‘contrast’ values (Equation 3). Thus, in this study, we use the mean “contrast” data at d=1 in the four directions (θ=0°, 45°, 90°, and 135°) to identify convective clouds.

Besides this parameter, we also employ the visible reflectance (VIS, 0.64 μm) and brightness temperatures (T_b) at 11.2 μm and 12.4 μm to help identify the distinctive patterns of convective clouds. The spatial gradient of T_b (11.2 μm) helps exclude very low-elevation fogs, whose temperatures are close to that of the surface in the morning. We use these three parameters in a k-means clustering analysis. Those clusters with relatively higher “contrast” (with mean Contrast>3.5) are considered either small convective clouds or the edges of mature convective clouds.

Unlike stratus clouds produced by large-scale systems, mature local convective cloud tops tend to have very high VIS reflectance and small area (Lima and Wilson, 2008). As the cloud tops of mature convective clouds are also relatively flat, they produce small “contrast” values. We consider those clusters having area smaller than 40,000 km^2 (10,000 pixels), mean VIS reflectance larger than 0.75, and maximum VIS reflectance larger than 0.9 as the tops of mature convective clouds.

In addition, we adopt the split window technique to exclude cirrus (Mecikalski and Bedka, 2006). The brightness temperature differences between 11.2 μm and 12.4 μm are near-zero for convective clouds, and we exclude those pixels with brightness temperature differences numerically smaller than -4K. This allows us to produce a cloud mask with a high probability of isolating convective cloud. Figure 2 shows the entire flowchart of our convective-cloud identification method.

As we identify convective clouds using the combined results from texture analysis, clustering, and thresholding, we name this cloud identification method the Texture-Clustering-Thresholding-Convection IDentification (TCT-CID) method.

3.2 Validation of the convective cloud mask

To validate the TCT-CID method, we compare the convective clouds identified with our cloud mask against the MODIS/Aqua MYD35 cloud mask. As the MODIS product does not classify clouds into different types, we use a scene from the hilly regions in southern China at 13:40 LT on July 30th, 2016 as an example. It contains a vast convective cloud field, and most of the clouds in this scene are convective clouds. Figure 3a shows the true-color image of the scene we chose. Figures 3b and 3c are the MODIS cloud mask data and the convective cloud mask from our method, respectively. We can see that there is a good agreement between the MODIS cloud mask and that identified by our method. As we have screened the cirrus with the split-window method to isolate only convective clouds, the cloud area identified by our method is smaller than the cloudy area found by the MODIS cloud mask. Nevertheless, the majority of convective clouds are well captured by our method.

In order to validate the result of convective clouds identified by the TCT-CID method statistically, we compared the identified convective cloud mask with the Himawari-8 Level 2 cloud type data from the L2CLP010 product (see https://www.eorc.jaxa.jp/ptree/userguide.html; last accessed: May 2020). This product provides the cloud type information using the ISCCP cloud classification criteria. The frequencies of different cloud types corresponding to the identified convective cloud masks are shown in Figure S1. We can find that the frequencies of DCC and Sc are relatively significant, especially around noon time, which indicates that the TCT-CID method is effective at identifying deep convective clouds and stratocumulus clouds. Other cloud types, such as altostratus, nimbostratus and cumulus cloud also show relatively large amounts. These cloud types can be seen as representing different stages in the development of convective clouds. Although their frequencies only exceed the median but not the 2σ values of the distributions, they still show significant differences from the frequency of cirrus, stratocirrus, altocumulus and stratus. After 16:00, as the solar zenith angle grows, the cloud top reflectance increases significantly. The criteria

https://doi.org/10.5194/acp-2020-845
Preprint. Discussion started: 13 October 2020

of the TCT-CID method become less strict, so that cloud identification errors increase. Nevertheless, the frequency of DCC still passes the 2σ line, which implies that deep convection is the most robust cloud type that can be identified by the TCT-CID method.

These results suggest that the identification by the TCT-CID method is relatively reliable in studying the convective cloud properties and their relationship with aerosols.

4. Results and discussion

4.1 The diurnal cycle of convective clouds

We use the L1 data from Himawari-8 acquired from May to September in 2016 and 2017 to identify local convective clouds over eastern China and build the spatial distribution of convective clouds. Figure 4 shows the frequency of convective clouds occurring between 08:00 and 17:00 LT, aggregated over the entire study period. This includes 20455 Himawari images, containing more than 2000 samples within each pixel within each hour. Convective cloud occurs predominantly over the sea in the morning, and gradually shifts inland after local noon. This convective cloud occurrence pattern is driven by distinct differences in the specific heat capacities and boundary-layer thermodynamics over land and ocean. In the morning, radiative cooling and land-breeze contribute to the formation of convective clouds over the ocean, whereas temperatures near the land surface tend to be relatively low, which makes it difficult for convective clouds to form there at this time of the day. But in the afternoon local time, as land surface temperatures increase, the near-surface air layer becomes more unstable, making it easier for convective clouds to form. The accumulation of land-surface heating during the day also favors the development of deep convection in the afternoon. Such patterns are highly consistent with previous studies (Garreaud and Wallace, 1997;Sui et al., 1997;Li et al., 2010).

To further validate the identification results, the statistical patterns of convective cloud masks are investigated in Figure 4 and 5. The impact of diurnal solar radiation variation and topography on convective clouds are already well-understood (Houze Jr.,

https://doi.org/10.5194/acp-2020-845
Preprint. Discussion started: 13 October 2020

1993;Houze Jr., 2012;2014), and thus, these results serve as further support for our cloud identification method. The gray lines in Figure 4 mark the 1000 m surface elevation contour, which is approximately the boundary between the plains and elevated terrains. Around 13:00-14:00 local time, convective clouds begin to form over the elevated regions, and the amount begins to increase afterwards (Figure 4).

Figure 5 shows the joint distribution of convective cloud occurrence frequency (CC OF) with respect to terrain height (TH) over land and associated meteorological factors. Vertical velocities (relative humidity) at 850 hPa and 925 hPa (700 hPa and 850 hPa) are used as proxies for the basic state of dynamics and water vapor for regions with elevation above and below 1000 m, respectively.

Generally, CC OF has two peaks, at heights below 500 m and above 1000 m (Figure 5a-d), which is likely due to the different sample sizes over terrain of different heights (Figure S2). Nevertheless, the thermal factors that impact convective cloud occurrence show strong differences between lower and higher elevation surfaces. Convective clouds tend to require more unstable thermal conditions over regions with higher surface elevation compared to regions with lower surface elevation (TH≤1000 m). The LTS can be 5~10K lower, whereas the potential temperature θ can be nearly 10K higher, for convective clouds to be favored at higher elevations. Further, instability and surface heating are also stronger when convective cloud occurrence is favored after about 11:00 LT relative to the early morning. For dynamical conditions, shown in Figure 5i-p, the mean values of CC OF for both ω_{850} and ω_{925} are negative (i.e., upward motion) and tend to move slightly in the negative direction and become stronger from 08:00-14:00, acting as a nonnegligible contributor to the diurnal variation of convective clouds during the day.

The under-cloud relative humidity (RH) values (RH_{700} and RH_{850} for regions of TH>1000 m and TH≤1000 m, respectively) show a general increase from 08:00 to 14:00 and are close to 100% when cloud occurrence is most common. In addition, the

https://doi.org/10.5194/acp-2020-845
Preprint. Discussion started: 13 October 2020

Atmospheric Chemistry and Physics Discussions

under-cloud RH over lower terrain is always higher than it is over higher-altitude regions during daytime (Figure 5q-x). This pattern may be caused by the stronger surface heating over higher terrain, which decreases the RH near the surface. Also note that where convective clouds occur, specific humidity at the surface (q) is always higher for regions having TH≤1000 m than for regions where TH>1000 m (Figure 5y-z2). This might indicate that, compared with higher terrain regions, it is always moister over lower terrain, so it is more difficult for cloud droplets to evaporate in such places. q over regions with TH>1000 m decreases more rapidly than for lower altitude regions from 11:00 to 17:00, but RH_{700} increases at higher altitudes, probably indicating that moisture over higher terrain is transported to higher altitudes to form convective clouds at these times.

All these thermal, dynamical and moisture conditions show relatively significant differences between lower and higher terrains in our data, which may reflect distinct impacts of topography on the formation and development of convective clouds. Such patterns show that our data conform to the expected patterns supports their use for the analysis presented below.

4.2 Changes in convective cloud diurnal cycle associated with aerosol

In this study, $PM_{2.5}$ observations from 1205 stations over eastern China are used as proxies for CCN, to roughly separate clouds into polluted and clean classes. We match the hourly measured $PM_{2.5}$ with the 10 min convective cloud identification results by supposing the convective cloud observed in the same hour occurs under the same $PM_{2.5}$ conditions. For each site, we use the top quarter of the $PM_{2.5}$ concentration distribution as the criterion for identifying polluted cases, and the bottom quarter as the clean cases (Figure 6). We then aggregate them into a 0.4°×0.4° grid using nearest neighbor interpolation. Only those clouds with centroids located within a grid box classified as polluted (clean) are deemed as polluted (clean) convective clouds. We calculated the convective cloud fraction (CCF) using the number of convective clouds under polluted (or clean) conditions divided by the total convective cloud amount within each grid cell.

https://doi.org/10.5194/acp-2020-845
Preprint. Discussion started: 13 October 2020

On average, 4.6×10^7 (4.1×10^7) pixels are deemed as clean (polluted) convective cloud within each hour. Figure 7 shows the difference of CCF in polluted and clean environments. Warm (cold) colors in the figure mean that there are more (less) convective clouds under the polluted condition. Additionally, only those data points that exceed the 95% significance level according to the Pearson's χ^2 test are plotted. From Figure 7a to 7e, we find that before 12:00 LT, convective clouds under polluted conditions generally occur in larger amounts, especially over the plateau region and some of the mountain regions. This pattern reverses gradually from 13:00 to 17:00 LT (Figure 7f-7j): the amount of convective clouds under polluted conditions tends to diminish, relative to those in clean conditions, in the afternoon. However, in several places, the CCF difference generally persists from morning to afternoon. Some red dots in southern and eastern China seem to occur over megacities, presumably caused by the co-action of high aerosol loading and the urban heat island effect (e.g., for the megacities around Yangtze River Delta (YRD) and the Pearl River Delta (PRD), marked by black circles in the figure). Furthermore, complex topography may also lead to different convective cloud response to aerosol loading. Over northern China, more convective clouds form over mountains under polluted conditions, whereas over the central China plain, with mountains around, convective clouds may be suppressed all the time by high aerosol loading. The number distribution of convective cloud clusters in each area bin, aggregated over the entire ROI is shown in Figure S3. Polluted convective cloud covers a larger area than clean convective cloud early in the day; this pattern gradually reverses after 13:00 LT, starting from the decrease in number of smaller convective cloud clusters. And after 14:00 LT, convective cloud area under clean conditions dominates. This pattern may suggest that high aerosol loading is probably one of the factors inhibiting the formation of small convective clouds via the aerosol radiative effect in the afternoon.

In an attempt to assess the effects of pollution on diurnal convective cloud behavior, the influence of other meteorological factors is addressed later in section 4.4 by

https://doi.org/10.5194/acp-2020-845
Preprint. Discussion started: 13 October 2020

stratifying the data based on such factors. We note here only that a relatively clear diurnal pattern in CCF exists, and that pollution effects appear to be correlated with this pattern.

Koren et al. (2008) demonstrated two opposite effects of absorbing aerosol on cloud cover, i.e. the microphysical effect and the radiation effect, by theoretical derivation, and verified this theory with observations in the Amazon region. Their study concluded that aerosol particles can increase cloud droplet number by serving as CCN. However, when aerosol concentration is higher, the attenuation of solar radiation by aerosol particles decreases the surface temperature, and atmospheric heating inhibits moisture flux, thus suppressing convection. As aerosol loading increases, surface temperature tends to decrease regardless of aerosol type (Gu et al., 2006;Jiang et al., 2013;Yang et al., 2016a;Yang et al., 2016b;Yang et al., 2018). Thus, we can infer that under conditions of high aerosol loading, the vertical moisture flux may be suppressed, which would inhibit convective cloud formation. Therefore, investigating the diurnal variation of aerosol microphysical and radiative effects might help explain the patterns shown in Figure 7.

Figure 8 shows the relationship between convective cloud and $PM_{2.5}$ concentration. Ten equally sampled bins of $PM_{2.5}$ concentration were defined, and we calculated the mean CCF within each bin using the convective cloud amount in each $PM_{2.5}$ bin divided by the total convective cloud amount within the same area for all $PM_{2.5}$ values. Sample sizes are shown in the color shaded background in each subfigure, and the mean sample number within each $PM_{2.5}$ bin is $\sim 8\times10^5$. The three-point moving average of the values is also plotted. We find that CCF first increases with respect to $PM_{2.5}$ mass concentration and then starts to decrease; this pattern persists throughout the day. The $PM_{2.5}$ mass concentrations at all turning points of the curves are between 20 μg/m^3 and 30 μg/m^3. Similar results were also found by previous studies (Guo et al., 2017;Jiang et al., 2018;Wang et al., 2018). Adding to these previous results, we find that the relationship

https://doi.org/10.5194/acp-2020-845
Preprint. Discussion started: 13 October 2020

of $PM_{2.5}$ and CCF persists throughout the day, as we have used high-resolution geostationary satellite data that provide us ample samples at different times. Furthermore, the aerosol effect on convective cloud is probably robust not only for deep convective clouds, but also for convective clouds at any stage of development. This pattern might be attributed to the competition between the microphysical effect dominating at low $PM_{2.5}$ concentration, and the radiative effect becoming increasingly important at higher $PM_{2.5}$ concentration.

The CCF values corresponding to the average thresholds identifying clean and polluted conditions (marked as vertical red line pairs with numbers in each Figure 8 panel) generally tend to be higher under polluted than under clean conditions from 08:00-11:00 LT, whereas from 12:00-17:00 LT the pattern gradually reverses. The shapes of the moving average curves change slightly from morning to afternoon compared with the mean CCF over all times (magenta dots), where CCF is lower in the morning before the tipping point but higher in the afternoon, and after the tipping point, CCF is higher in the morning but lower in the afternoon. As we found from Figures 5 and 7, meteorological condition changes associated with topography and diurnal solar radiation variations may play roles in altering the shapes of the CCF curves. For conditions with $PM_{2.5}$ concentrations lower than the 20~30 $\mu g/m^3$ turning zone, more convective cloud is formed, probably due to more unstable environments and stronger surface heating, especially in the afternoon. But as the surface is generally moister before noon time (Figure 5x-z2), especially at higher terrains, the higher q may suppress cloud droplet evaporation and thus keep CCF from sharply decreasing.

4.3 Effects of topography on the aerosol-convective-cloud relationship

In order to isolate the probable effect of topography on the aerosol-convective-cloud relationship, we further investigate in this section the CCF changes along with TH at different levels of aerosol loading. The mean CCFs at different TH in both polluted and clean conditions are shown in Figure 9. The CCF under clean (or polluted) conditions is calculated using the formula shown below:

https://doi.org/10.5194/acp-2020-845
Preprint. Discussion started: 13 October 2020

$$\mathrm{CCF}_{C(P)}(i,j;h,t) = \frac{N_{C(P)}(i,j;h,t)}{N_{total}(i,j;h)} \times 100\% \tag{7}$$

where $N_{C(P)}(i,j;h,t)$ represents the number of convective clouds occurring under clean (C) or polluted (P) conditions in the $(i,j)^{th}$ pixel box in ROI in elevation bin h during hour t, and $N_{total}(i,j;h)$ represents the total number of convective clouds observed in each pixel box at elevation bin h during the daytime. Sample sizes are shown in Figure S2. We find that the CCF difference between polluted and clean conditions generally agrees with Figure 7 in that CCF is higher for polluted cases in the morning, lower in the afternoon, and the differences are statistically greatest in early morning and late afternoon. In addition, the CCF differences between polluted and clean conditions vary considerably along with increasing TH, which may indicate that the effects of topography and air quality on CCF co-vary, and the impact of topography might be much stronger compared with increased aerosol loading.

There is also another aspect of these phenomena. In Figure 10, by normalizing the occurrence frequencies by the total number of polluted and clean cases within each hour, respectively, we explore how topography changes the polluted and clean convective clouds spatially. The formula for this normalized CCF (NCCF) can be written:

$$\mathrm{NCCF}_{C(P)}(i,j;h,t) = \frac{N_{C(P)}(i,j;h,t)}{\sum_i \sum_j N_{C(P)}(i,j;h,t)} \times 100\% \tag{8}.$$

The mean NCCF is calculated within each elevation bin h. Unlike CCF (Equation 7), the denominator for NCCF (Equation 8) is not summed over all times-of-day; because the elevation-related response reverses over the day (e.g., Figure 9), NCCF focuses more specifically on how CCF at a given location and terrain elevation compares with all locations at the same elevation and the same time, reducing the influence of diurnal variation and emphasizing elevation-related differences. As such, the difference in NCCF between clean and polluted cases reflects the difference caused by topography when the overall environment is under clean or polluted conditions. We can see from Figure 11 that below the elevation of 500 m, most of the convective clouds are

https://doi.org/10.5194/acp-2020-845
Preprint. Discussion started: 13 October 2020

Atmospheric Chemistry and Physics Discussions

suppressed under polluted conditions, whereas over regions with terrain height greater than 1000 m, especially before 14:00 LT, the amount of convective cloud under polluted conditions is significantly larger. This phenomenon may partly explain the results shown in Figure 7, where complex topography plays an important role in the aerosol effect on convective clouds. Under polluted conditions, convective clouds over lower terrain are much easier to suppress, whereas over elevated terrain, convective clouds are more likely to be invigorated.

As the topography over eastern China has a general step-like distribution, we roughly separate the terrain heights into four bins representing the plains (0-500 m), mountain ranges (500-1000 m), plateau (1000-1500 m) and high mountains (1500-2000 m), and assess how the aerosol effect changes over different topography. The pixel number within each bin is over 4.0×10^5,1.6×10^5.2.3×10^5 and 0.5×10^5. We calculate the CCF within each of the 10 equally sampled $PM_{2.5}$ bins over each sub-region. Figure 11 shows how cloud fraction changes with respect to $PM_{2.5}$ concentration over the four different terrain elevation ranges. In all four sub-regions, CCF first increases with $PM_{2.5}$ concentration and then decreases. But before the turning zone (between 20~30 $\mu g/m^3$) the CCF is slightly higher over mountains and plateaus than over the plains, but after the turning zone, this pattern reverses. This probably occurs because instability and surface heating are stronger over the higher terrain, which invigorates the convective cloud development by enhancing the aerosol microphysical effect (Rosenfeld and Lohmann, 2008). The air over the plain regions is moister than that over the mountain and plateau regions, which suppresses droplet evaporation thus tends to overtake the aerosol radiative effect.

In order to further investigate the probable effect of topography in aerosol-convective-cloud relationship, the vertical circulation and moisture distributions are studied. The meridional-vertical distribution of relative humidity and wind are shown in Figure 12. Generally, the circulation pattern is consistent throughout the day, the

https://doi.org/10.5194/acp-2020-845
Preprint. Discussion started: 13 October 2020

updraft south to 35°N is always stronger than that over the northern region, and the relative humidity in this region is significantly higher. Under clean conditions, the strong updraft and southerly wind south to 30°N may bring large amount of moisture inland, contributing to convection development in this region. But under polluted conditions, the southerly wind is weaker, and the relative humidity above this region is lower, which may lead to a restraint of convective cloud development due to the inhibition of aerosol microphysical effect. In regions north to 35°N, there is an obvious north wind component under clean conditions, bringing dry and clean air to this region, which may suppress the development of convective clouds. But under polluted conditions, under the control of a relatively strong southerly wind, moisture and pollutants may be blown toward the mountain regions and forced to be uplifted by the elevated terrain, strengthening the formation and development of convective clouds, especially over the windward slopes north to 40°N. The zonal-vertical wind and relative humidity changes are shown in Figure S4 and S5. The updraft along windward slopes is always stronger, especially under polluted conditions in the northern part of the ROI. This is likely to contribute to strengthening the aerosol microphysical effect over such regions, which facilitates the invigoration of convective clouds. All the patterns described above agree well with the phenomena identified in the previous figures, indicating that different circulation patterns and the changes associated with different topography may have a considerable impact on the variability of the aerosol-convective-cloud relationship.

4.4 The environmental dependence of the aerosol effect

To further isolate the signal of aerosol effects from that of meteorological conditions, and to characterize the co-variation of topography and aerosol effects on convective clouds, the changes of CCF with aerosol loading under various thermodynamic, dynamical and humidity conditions at different time-of-day and over different terrain heights are shown in Figures 13 and 14. Note that vertical velocities (relative humidity) at 850 hPa and 925 hPa (700 hPa and 850 hPa) are used to represent the basic dynamics

https://doi.org/10.5194/acp-2020-845
Preprint. Discussion started: 13 October 2020

(water vapor) state for regions with elevation above and below 1000 m, respectively. We defined ten equally sampled bins of $PM_{2.5}$ concentration and calculated the joint distribution of CCF along with each $PM_{2.5}$ and meteorological factor bin, the sample sizes in each subfigure is shown in Table S1 and S2. Generally, the CCF along with $PM_{2.5}$ concentration shows unimodal distributions, CCFs increase at first and then decrease with $PM_{2.5}$ concentration, as we saw in Figure 8, but now in each of the vertical velocity and relative humidity strata, i.e., regardless of differences in meteorological conditions. The patterns are consistent at different time-of-day and over different topography, which may indicate that under different thermodynamic, dynamical and water vapor conditions the competition between the aerosol microphysical and radiation effects always exists, no matter how meteorological conditions vary, at least within the study domain.

The mean tipping point of CCF curves at different values of meteorological variables is marked as the turning line between the increasing and decreasing CCF trends (dashed lines in Figures 13 and 14). From Figure 13a-h, the turning line moves to smaller $PM_{2.5}$ values as surface heating increases and the atmosphere becomes more unstable from morning to late afternoon. The peaks of CCF move from stable (weak surface heating) conditions to unstable (strong surface heating) conditions during the day (Figure 13a-h and 14a-h). This phenomenon may prove that changes in thermodynamic conditions attributed to diurnal solar radiation variation and topography are probably among the impact factors that influence the changing CCF curve shapes in Figures 8 and 11. Stronger surface heating and more unstable conditions may increase CCF when the microphysical effect of aerosol dominates the CCF changes, and would probably strengthen the aerosol microphysical effect.

Updraft changes, which can represent under-cloud dynamical conditions, at 850 hPa and 925 hPa for terrain higher and lower than 1000 m, respectively, are relatively small during the day and over different topography. However, the turning values of CCF generally decrease and CCF peaks occur under stronger updraft conditions as well

(Figure 13i-p). This pattern may indicate that more aerosol particles are entrained into the clouds from the boundary layer when uplift is stronger, which in turn might strengthen the aerosol microphysical effect. Further, as shown in Figure 14k-l, stronger updrafts over higher mountains (with TH>1500 m) invigorate convective clouds after the turning line, especially for $PM_{2.5}$ concentrations higher than 50 μg/m^3, which suggests that the suppression of convective clouds by aerosol radiative effect is counteracted.

For water vapor conditions, both higher relative humidity below cloud base (Figures 13q-x and 14q-x) and higher specific humidity at surface (Figures 13y-z2 and 14y-z2) generally produce larger CCF. Higher RH and higher q are also associated with higher CCF peaks. These patterns indicate that moister conditions can lead to greater activation of aerosol particles, which may strengthen the aerosol microphysical effect, and might overtake the suppression from the aerosol radiative effect in higher aerosol loading conditions in these regions.

The meteorological factors that influence the aerosol effect on convective clouds are very likely to interact with one another, which may produce combined impacts on convective clouds and lead to nonlinear changes to the CCF distribution, creating large variations in the results. By analyzing the probable co-variation of aerosol effects, meteorological factors and the impact of topography on convective clouds, we find that the CCF changes caused by both the aerosol microphysical and radiative effects are robust under a range of meteorological conditions, whereas the strength of these two effects can be influenced by specific thermodynamic, dynamical and humidity conditions.

However, testing whether the results are due mainly to aerosol effects is only a first step; establishing proof of the mechanisms by which aerosol affects convective cloud occurrence is another important question. If synoptic factors, differences in meteorological conditions associated with topography and aerosols work together,

https://doi.org/10.5194/acp-2020-845
Preprint. Discussion started: 13 October 2020

Atmospheric Chemistry and Physics Discussions

determining which factors dominate the formation and development of convective clouds needs to be explored with deeper mining of the data, as well as modeling studies, in the future.

5. Summary

Following rapid economic development and industrialization, eastern China has faced increasingly severe air pollution during recent decades. Aerosols, which play an important role in the formation and development of clouds and precipitation, can be among the main factors influencing urban inundation, hail and severe storms.

The interaction between aerosol, weather, and topography is complex, so untangling their effects, that jointly influence convective cloud formation, is difficult. This study applies very large, diurnally resolved geostationary satellite data and extensive ground-based observations to investigate the characteristics of convective clouds, the impacts of aerosol on convective cloud properties, and the potential mechanisms that define the aerosol impacts on convective clouds under different meteorological conditions and over different topography. Having such large data sets allows us to stratify by various factors and isolate patterns among the multiple dimensions. The key results of this study are as follows:

- We develop a convective cloud identification process named the TCT-CID algorithm by combining the merits of texture analysis, a clustering technique, and a threshold method, using the Level 1 data from the Japanese geostationary satellite Himawari-8 during the period from May to September in 2016 and 2017. The method offers stable and relatively accurate performance in identifying convective clouds.
- The cloud mask is used to study the occurrence frequency and the regional distribution of convective clouds over eastern China, first to determine whether the

new data reproduce expected cloud-occurrence patterns. Statistical results show that convective cloud occurrence frequency (CC OF) is higher under more unstable conditions with stronger surface heating and updraft. And in the afternoon, this phenomenon is more significant than in the morning. The increases in both under-cloud relative humidity and surface specific humidity produce higher CC OF during the day. There is also a significant difference between higher and lower terrain regions. The consistency of these patterns with previous studies and the classic theories of convective cloud formation helps validate the results of the TCT-CID algorithm.

- We then compared convective clouds under clean and polluted conditions, and further examined the possible impact of the diurnal cycle and topography on the aerosol-convective-cloud relationship. We find that the convective cloud fraction generally tends to be larger before noon and smaller in the afternoon under more polluted conditions, but megacities and complex topography can influence the pattern. This result provides a new perspective on the aerosol effect compared to previous studies.
- A relationship between aerosol loading and convective cloud fraction is found. The cloud fraction increases initially, but then decreases with successive increases in aerosol loading. This pattern is likely due to the combined action of the aerosol microphysical and radiative effects. Previous studies found similar results for deep convective cloud and convective precipitation studies, but by using high-resolution geostationary satellite observations, we further find that this pattern is probably robust for convective clouds at all stages of development.
- Although the aerosol-convective-cloud relationship is relatively stable, some variability also exists. The pattern varies throughout the day depending on terrain height, and is modulated by varying thermodynamic, dynamical and humidity conditions during the day. We find that the meteorological variations driven by

diurnal solar radiation changes and topography are probably among the reasons for changes in the relative strength of aerosol microphysical and radiative effects. Over higher terrains such as mountains and plateaus, a southerly wind component is likely to contribute to the strengthening of the microphysical effect through forced uplifting of pollutant and moisture, which invigorates convective cloud over the windward slopes, whereas over plains areas, aerosol pollution blocking solar radiation is likely to dominate, thus decreasing the surface heating and suppressing convection by the enhancing the radiative effect. However, as aerosol concentration, synoptic meteorological factors and topography might work together in influencing the formation and development of convective cloud, the phenomena found above can also be affected by nonlinear interactions among these factors.

Moreover, the analysis of this study is based mainly on satellite observations, which in themselves provide limited insight into the mechanism underlying the observed patterns. In the current study, we aimed only to isolate the possible effects of aerosol on convective cloud properties under different meteorological conditions. However, further exploration, including model simulations and/or targeted in-situ or aircraft observations, are still needed to reveal the specific mechanisms behind these phenomena.

Acknowledgment

We acknowledge the JAXA P-tree system (http://www.eorc.jaxa.jp/ptree/) for providing the Himawari-8 Level 1 data, and the Global Modeling and Assimilation Office (GMAO) (https://gmao.gsfc.nasa.gov/reanalysis/MERRA-2/), for providing MERRA-2 reanalysis data. We would also like to extend our sincerest thanks and appreciation to the China National Environmental Monitoring Center for providing the hourly $PM_{2.5}$ data. This study is supported by the Natural Science Foundation of China (41925022, 91837204), the Ministry of Science and Technology of China National Key

https://doi.org/10.5194/acp-2020-845
Preprint. Discussion started: 13 October 2020

Atmospheric Chemistry and Physics Discussions

R&D Program on Monitoring, Early Warning and Prevention of Major Natural Disasters (2017YFC1501403).

https://doi.org/10.5194/acp-2020-845
Preprint. Discussion started: 13 October 2020

References

Ackerman, A. S., Toon, O. B., Stevens, D. E., Heymsfield, A. J., Ramanathan, V., and Welton, E. J.: Reduction of Tropical Cloudiness by Soot, Science, 288, 1042-1047, 10.1126/science.288.5468.1042, 2000.

Albrecht, B. A.: Aerosols, cloud microphysics, and fractional cloudiness, Science, 245, 1227, 1989.

Altaratz, O., Koren, I., Remer, L., and Hirsch, E.: Review: Cloud invigoration by aerosols—Coupling between microphysics and dynamics, Atmospheric Research, 140, 38-60, 2014.

Andreae, M. O., Rosenfeld, D., Artaxo, P., Costa, A. A., Frank, G. P., Longo, K. M., and Silva-Dias, M. A. F.: Smoking rain clouds over the Amazon, Science, 303, 1337-1342, 10.1126/science.1092779, 2004.

Andreae, M. O.: Correlation between cloud condensation nuclei concentration and aerosol optical thickness in remote and polluted regions, Atmospheric Chemistry and Physics, 9, 543-556, 2009.

Baum, B. A., Tovinkere, V., Titlow, J., and Welch, R. M.: Automated Cloud Classification of Global AVHRR Data Using a Fuzzy Logic Approach, Journal of Applied Meteorology, 36, 1519-1540, 10.1175/1520-0450(1997)036<1519:accoga>2.0.co;2, 1997.

Bessho, K., Date, K., Hayashi, M., Ikeda, A., Imai, T., Inoue, H., Kumagai, Y., Miyakawa, T., Murata, H., Ohno, T., Okuyama, A., Oyama, R., Sasaki, Y., Shimazu, Y., Shimoji, K., Sumida, Y., Suzuki, M., Taniguchi, H., Tsuchiyama, H., Uesawa, D., Yokota, H., and Yoshida, R.: An Introduction to Himawari-8/9— Japan’s New-Generation Geostationary Meteorological Satellites, Journal of the Meteorological Society of Japan. Ser. II, 94, 151-183, 10.2151/jmsj.2016-009, 2016.

Bottino, M. J., and Ceballos, J. C.: Daytime cloud classification over South American region using multispectral GOES-8 imagery, International Journal of Remote Sensing, 36, 1-19, 10.1080/01431161.2014.978953, 2014.

Chakraborty, S., Fu, R., Wright, J. S., and Massie, S. T.: Relationships between convective structure and transport of aerosols to the upper troposphere deduced from satellite observations, Journal of Geophysical Research: Atmospheres, 120, 6515-6536, 10.1002/2015jd023528, 2015.

Chakraborty, S., Fu, R., Massie, S. T., and Stephens, G.: Relative influence of meteorological conditions and aerosols on the lifetime of mesoscale convective systems, Proceedings of the National Academy of Sciences, 113, 7426-7431, www.pnas.org/cgi/doi/10.1073/pnas.1601935113, 2016.

Chakraborty, S., Schiro, K. A., Fu, R., and Neelin, J. D.: On the role of aerosols, humidity, and vertical wind shear in the transition of shallow-to-deep convection at the Green Ocean Amazon 2014/5 site, Atmospheric Chemistry and Physics, 18, 11135-11148, 10.5194/acp-18-11135-2018, 2018.

Chang, A. T. C., Chiu, L. S., and Yang, G.: Diurnal Cycle of Oceanic Precipitation from SSM/I Data, Monthly Weather Review, 123, 3371-3380, 10.1175/1520-0493(1995)123<3371:dcoopf>2.0.co;2, 1995.

Charlson, R. J., Schwartz, S. E., Hales, J. M., Cess, KLEY, J. A., Hansen, J. E., and Hofmann, D. J.: Climate Forcing by Anthropogenic Aerosols, Science, 255, 423-430, 10.1126/science.255.5043.423, 1992.

Chen, T. M., Guo, J. P., Li, Z. Q., Zhao, C. F., Liu, H., Cribb, M., Wang, F., and He, J.: A CloudSat Perspective on the Cloud Climatology and Its Association with Aerosol Perturbations in the Vertical over Eastern China, Journal of the Atmospheric Sciences, 73, 3599-3616, 10.1175/jas-d-15-0309.1,

https://doi.org/10.5194/acp-2020-845
Preprint. Discussion started: 13 October 2020

2016.

Fan, J., Leung, L. R., Rosenfeld, D., Chen, Q., Li, Z., Zhang, J., and Yan, H.: Microphysical effects determine macrophysical response for aerosol impacts on deep convective clouds, Proceedings of the National Academy of Sciences, 110, E4581-E4590, 10.1073/pnas.1316830110, 2013.

Fan, J., Rosenfeld, D., Yang, Y., Zhao, C., Leung, L. R., and Li, Z.: Substantial contribution of anthropogenic air pollution to catastrophic floods in Southwest China, Geophysical Research Letters, 42, 6066-6075, 10.1002/2015gl064479, 2015.

Feingold, G., Eberhard, W. L., Veron, D. E., and Previdi, M.: First measurements of the Twomey indirect effect using ground-based remote sensors, Geophysical Research Letters, 30, doi:10.1029/2002GL016633, 2003.

Feingold, G., Jiang, H. L., and Harrington, J. Y.: On smoke suppression of clouds in Amazonia, Geophysical Research Letters, 32, L02804, 10.1029/2004gl021369, 2005.

Garreaud, R., and Wallace, J. M.: The Diurnal March of Convective Cloudiness over the Americas, Monthly Weather Review, 125, 3157-3171, 10.1175/1520-0493(1997)125<3157:tdmocc>2.0.co;2, 1997.

Garrett, T. J., Zhao, C., Dong, X., Mace, G. G., and Hobbs, P. V.: Effects of varying aerosol regimes on low-level Arctic stratus, Geophysical Research Letters, 31, L17105, 10.1029/2004gl019928, 2004.

Garrett, T. J., and Zhao, C.: Increased Arctic cloud longwave emissivity associated with pollution from mid-latitudes, Nature, 440, 787-789, 2006.

Gelaro, R., McCarty, W., Suárez, M. J., Todling, R., Molod, A., Takacs, L., Randles, C. A., Darmenov, A., Bosilovich, M. G., Reichle, R., Wargan, K., Coy, L., Cullather, R., Draper, C., Akella, S., Buchard, V., Conaty, A., Silva, A. M. d., Gu, W., Kim, G.-K., Koster, R., Lucchesi, R., Merkova, D., Nielsen, J. E., Partyka, G., Pawson, S., Putman, W., Rienecker, M., Schubert, S. D., Sienkiewicz, M., and Zhao, B.: The Modern-Era Retrospective Analysis for Research and Applications, Version 2 (MERRA-2), Journal of Climate, 30, 5419-5454, 10.1175/jcli-d-16-0758.1, 2017.

Givati, A., and Rosenfeld, D.: Quantifying Precipitation Suppression Due to Air Pollution, Journal of Applied Meteorology, 43, 1038-1056, 10.1175/1520-0450(2004)043<1038:qpsdta>2.0.co;2, 2004.

Gryspeerdt, E., and Stier, P.: Regime-based analysis of aerosol-cloud interactions, Geophysical Research Letters, 39, L21802, 10.1029/2012gl053221, 2012.

Gryspeerdt, E., Stier, P., and Partridge, D. G.: Satellite observations of cloud regime development: the role of aerosol processes, Atmospheric Chemistry and Physics, 14, 1141-1158, 10.5194/acp-14-1141-2014, 2014.

Gu, Y., Liou, K. N., Xue, Y., Mechoso, C. R., Li, W., and Luo, Y.: Climatic effects of different aerosol types in China simulated by the UCLA general circulation model, Journal of Geophysical Research: Atmospheres, 111, 10.1029/2005jd006312, 2006.

Guo, J., Zhang, X., Wu, Y.-r., Zhaxi, Y., Che, H., La, B., Wang, W., and Li, X.: Spatio-temporal variation trends of satellite-based aerosol optical depth in China during 1980–2008, Atmospheric Environment, 45, 6802-6811, 10.1016/j.atmosenv.2011.03.068, 2011.

Guo, J., Deng, M., Lee, S. S., Wang, F., Li, Z., Zhai, P., Liu, H., Lv, W., Yao, W., and Li, X.: Delaying precipitation and lightning by air pollution over the Pearl River Delta. Part I: Observational analyses, Journal of Geophysical Research: Atmospheres, 121, 6472-6488, 10.1002/2015jd023257, 2016.

Guo, J., Su, T., Li, Z., Miao, Y., Li, J., Liu, H., Xu, H., Cribb, M., and Zhai, P.: Declining frequency of summertime local-scale precipitation over eastern China from 1970 to 2010 and its potential link to

https://doi.org/10.5194/acp-2020-845
Preprint. Discussion started: 13 October 2020

Atmospheric Chemistry and Physics Discussions

aerosols, Geophysical Research Letters, 44, 5700-5708, 10.1002/2017gl073533, 2017.

Guo, J., Liu, H., Li, Z., Rosenfeld, D., Jiang, M., Xu, W., Jiang, J. H., He, J., Chen, D., Min, M., and Zhai, P.: Aerosol-induced changes in the vertical structure of precipitation: a perspective of TRMM precipitation radar, Atmos. Chem. Phys., 18, 13329-13343, 10.5194/acp-18-13329-2018, 2018.

Haralick, R. M., Shanmugam, K., and Dinstein, I.: Textural Features for Image Classification, IEEE Transactions on Systems, Man, and Cybernetics, SMC-3, 610-621, 10.1109/TSMC.1973.4309314, 1973.

Haralick, R. M.: Statistical and structural approaches to texture, Proceedings of the IEEE, 67, 786-804, 10.1109/PROC.1979.11328, 1979.

Houze Jr., R. A.: Cloud Dynamics, Academic Press, Inc., 1993.

Houze Jr., R. A.: Orographic effects on precipitating clouds, Reviews of Geophysics, 50, 10.1029/2011rg000365, 2012.

Houze Jr., R. A.: Cloud dynamics, Academic press, 2014.

Jiang, J. H., Su, H., Huang, L., Wang, Y., Massie, S. T., Zhao, B., Omar, A., and Wang, Z.: Contrasting effects on deep convective clouds by different types of aerosols, Nature Communications, 9, 7, 10.1038/s41467-018-06280-4, 2018.

Jiang, Y., Liu, X., Yang, X.-Q., and Wang, M.: A numerical study of the effect of different aerosol types on East Asian summer clouds and precipitation, Atmospheric Environment, 70, 51-63, https://doi.org/10.1016/j.atmosenv.2012.12.039, 2013.

Kaufman, Y. J., and Nakajima, T.: EFFECT OF AMAZON SMOKE ON CLOUD MICROPHYSICS AND ALBEDO - ANALYSIS FROM SATELLITE IMAGERY, Journal of Applied Meteorology, 32, 729-744, 10.1175/1520-0450(1993)032<0729:eoasoc>2.0.co;2, 1993.

Kaufman, Y. J., Tanre, D., and Boucher, O.: A satellite view of aerosols in the climate system, Nature, 419, 215-223, 2002.

Kaufman, Y. J., Koren, I., Remer, L. A., Rosenfeld, D., and Rudich, Y.: The effect of smoke, dust, and pollution aerosol on shallow cloud development over the Atlantic Ocean, Proceedings of the National Academy of Sciences, 102, 11207-11212, 10.1073/pnas.0505191102, 2005.

Khain, A., Rosenfeld, D., and Pokrovsky, A.: Aerosol impact on the dynamics and microphysics of deep convective clouds, Quarterly Journal of the Royal Meteorological Society, 131, 2639-2663, 2005.

Kirshbaum, D. J., and Durran, D. R.: Factors Governing Cellular Convection in Orographic Precipitation, Journal of the Atmospheric Sciences, 61, 682-698, 10.1175/1520-0469(2004)061<0682:fgccio>2.0.co;2, 2004.

Kirshbaum, D. J., and Durran, D. R.: Atmospheric Factors Governing Banded Orographic Convection, Journal of the Atmospheric Sciences, 62, 3758-3774, 10.1175/jas3568.1, 2005.

Kirshbaum, D. J., Bryan, G. H., Rotunno, R., and Durran, D. R.: The Triggering of Orographic Rainbands by Small-Scale Topography, Journal of the Atmospheric Sciences, 64, 1530-1549, 10.1175/jas3924.1, 2007.

Klein, S. A., and Hartmann, D. L.: The Seasonal Cycle of Low Stratiform Clouds, Journal of Climate, 6, 1587-1606, 10.1175/1520-0442(1993)006<1587:tscols>2.0.co;2, 1993.

Koren, I., Martins, J. V., Remer, L. A., and Afargan, H.: Smoke invigoration versus inhibition of clouds over the Amazon, Science, 321, 946-949, 10.1126/science.1159185, 2008.

Lee, J. M., Zhang, Y., and Klein, S. A.: The Effect of Land Surface Heterogeneity and Background Wind on Shallow Cumulus Clouds and the Transition to Deeper Convection, Journal of the Atmospheric

https://doi.org/10.5194/acp-2020-845
Preprint. Discussion started: 13 October 2020

Sciences, 76, 401-419, 10.1175/jas-d-18-0196.1, 2019.

Li, W., Luo, C., Wang, D., and Lei, T.: Diurnal variations of precipitation over the South China Sea, Meteorology and Atmospheric Physics, 109, 33-46, 10.1007/s00703-010-0094-8, 2010.

Li, Z. and D. Weng.: A model to determine topographic parameters, Acta Geographica Sinica, 42, 269-278, 1987.

Li, Z., and D. Weng.: A computer model for calculating the duration of sunshine in mountainous areas, Chinese Science Bulletin, 33, 1624-1627, 1988.

Li, Z., and D. Weng.: A numerical model for hilly-land global radiation, Acta Meteorologica Sinica, 3, 661-668, 1989.

Li, Z., Zhao, X., Kahn, R., Mishchenko, M., Remer, L., Lee, K.-H., M.Wang, Laszlo, I., Nakajima, T., and Maring, H.: Uncertainties in satellite remote sensing of aerosols and impact on monitoring its long-term trend: a review and perspective, Annales Geophysicae, 27, 2755-2770, 2009.

Li, Z., Niu, F., Fan, J., Liu, Y., Rosenfeld, D., and Ding, Y.: Long-term impacts of aerosols on the vertical development of clouds and precipitation, Nature Geoscience, 4, 888-894, 10.1038/ngeo1313, 2011.

Li, Z., Lau, W. K. M., Ramanathan, V., Wu, G., Ding, Y., Manoj, M. G., Liu, J., Qian, Y., Li, J., Zhou, T., Fan, J., Rosenfeld, D., Ming, Y., Wang, Y., Huang, J., Wang, B., Xu, X., Lee, S. S., Cribb, M., Zhang, F., Yang, X., Zhao, C., Takemura, T., Wang, K., Xia, X., Yin, Y., Zhang, H., Guo, J., Zhai, P. M., Sugimoto, N., Babu, S. S., and Brasseur, G. P.: Aerosol and monsoon climate interactions over Asia, Reviews of Geophysics, 54, 866-929, 10.1002/2015rg000500, 2016.

Li, Z., Wang, Y., Guo, J., Zhao, C., Cribb, M. C., Dong, X., Fan, J., Gong, D., Huang, J., Jiang, M., Jiang, Y., Lee, S.-S., Li, H., Li, J., Liu, J., Qian, Y., Rosenfeld, D., Shan, S., Sun, Y., Wang, H., Xin, J., Yan, X., Yang, X., Yang, X.-q., Zhang, F., and Zheng, Y.: East Asian Study of Tropospheric Aerosols and their Impact on Regional Clouds, Precipitation, and Climate (EAST-AIRCPC), Journal of Geophysical Research-Atmospheres, 124, 10.1029/2019jd030758, 2019.

Lima, M. A., and Wilson, J. W.: Convective Storm Initiation in a Moist Tropical Environment, Monthly Weather Review, 136, 1847-1864, 10.1175/2007mwr2279.1, 2008.

Lohmann, U., and Feichter, J.: Global indirect aerosol effects: a review, Atmos. Chem. Phys., 5, 715-737, 10.5194/acp-5-715-2005, 2005.

Lynn, B., Khain, A., Rosenfeld, D., and Woodley, W. L.: Effects of aerosols on precipitation from orographic clouds, Journal of Geophysical Research: Atmospheres, 112, 10.1029/2006jd007537, 2007.

McCormick, R. A., and Ludwig, J. H.: Climate Modification by Atmospheric Aerosols, Science, 156, 1358-1359, 10.1126/science.156.3780.1358, 1967.

Mecikalski, J. R., and Bedka, K. M.: Forecasting convective initiation by monitoring the evolution of moving cumulus in daytime GOES imagery, Monthly Weather Review, 134, 49-78, 10.1175/mwr3062.1, 2006.

Niu, F., and Li, Z.: Systematic variations of cloud top temperature and precipitation rate with aerosols over the global tropics, Atmospheric Chemistry and Physics, 12, 8491-8498, 10.5194/acp-12-8491-2012, 2012.

Purdom, J. F. W.: Some Uses of High-Resolution GOES Imagery in the Mesoscale Forecasting of Convection and Its Behavior, Monthly Weather Review, 104, 1474-1483, 10.1175/1520-0493(1976)104<1474:suohrg>2.0.co;2, 1976.

Qiu, Y., Zhao, C., Guo, J., and Li, J.: 8-Year ground-based observational analysis about the seasonal

https://doi.org/10.5194/acp-2020-845
Preprint. Discussion started: 13 October 2020

variation of the aerosol-cloud droplet effective radius relationship at SGP site, Atmospheric Environment, 164, 139-146, https://doi.org/10.1016/j.atmosenv.2017.06.002, 2017.

Ramanathan, V., Crutzen, P. J., Kiehl, J. T., and Rosenfeld, D.: Aerosols, Climate, and the Hydrological Cycle, Science, 294, 2119-2124, 10.1126/science.1064034, 2001.

Redelsperger, J.-L., Parsons, D. B., and Guichard, F.: Recovery Processes and Factors Limiting Cloud-Top Height following the Arrival of a Dry Intrusion Observed during TOGA COARE, Journal of the Atmospheric Sciences, 59, 2438-2457, 10.1175/1520-0469(2002)059<2438:rpaflc>2.0.co;2, 2002.

Roe, G. H.: OROGRAPHIC PRECIPITATION, Annual Review of Earth and Planetary Sciences, 33, 645-671, 10.1146/annurev.earth.33.092203.122541, 2005.

Romatschke, U., and Jr., R. A. H.: Extreme Summer Convection in South America, Journal of Climate, 23, 3761-3791, 10.1175/2010jcli3465.1, 2010.

Romatschke, U., Medina, S., and Jr., R. A. H.: Regional, Seasonal, and Diurnal Variations of Extreme Convection in the South Asian Region, Journal of Climate, 23, 419-439, 10.1175/2009jcli3140.1, 2010.

Romatschke, U., and Jr., R. A. H.: Characteristics of Precipitating Convective Systems in the Premonsoon Season of South Asia, Journal of Hydrometeorology, 12, 157-180, 10.1175/2010jhm1311.1, 2011a.

Romatschke, U., and Jr., R. A. H.: Characteristics of Precipitating Convective Systems in the South Asian Monsoon, Journal of Hydrometeorology, 12, 3-26, 10.1175/2010jhm1289.1, 2011b.

Rosenfeld, D.: Suppression of Rain and Snow by Urban and Industrial Air Pollution, Science, 287, 1793-1796, 10.1126/science.287.5459.1793, 2000.

Rosenfeld, D., and Givati, A.: Evidence of Orographic Precipitation Suppression by Air Pollution–Induced Aerosols in the Western United States, Journal of Applied Meteorology and Climatology, 45, 893-911, 10.1175/jam2380.1, 2006.

Rosenfeld, D., Lohmann, U., Raga, G. B., O'Dowd, C. D., Kulmala, M., Fuzzi, S., Reissell, A., and Andreae, M. O.: Flood or Drought: How Do Aerosols Affect Precipitation?, Science, 321, 1309-1313, 2008.

Rosenfeld, D., and Ulrike Lohmann, G. B. R., Colin D. O'Dowd, Markku Kulmala, Sandro Fuzzi, Anni Reissell, Meinrat O. Andreae: Flood or Drought: How Do Aerosols Affect Precipitation?, Science, 321, 1309-1313, 10.1126/science.1160606, 2008.

Rosenfeld, D., Andreae, M. O., Asmi, A., Chin, M., de Leeuw, G., Donovan, D. P., Kahn, R., Kinne, S., Kivekäs, N., Kulmala, M., Lau, W., Schmidt, K. S., Suni, T., Wagner, T., Wild, M., and Quaas, J.: Global observations of aerosol-cloud-precipitation-climate interactions, Reviews of Geophysics, 52, 1-59, 10.1002/2013rg000441, 2014a.

Rosenfeld, D., Sherwood, S., Wood, R., and Donner, L. J.: Climate Effects of Aerosol-Cloud Interactions, Science, 343, 379-380, 10.1126/science.1247490, 2014b.

Stevens, B., and Feingold, G.: Untangling aerosol effects on clouds and precipitation in a buffered system, Nature, 461, 607, 10.1038/nature08281, 2009.

Sui, C.-H., Lau, K.-M., Takayabu, Y. N., and Short, D. A.: Diurnal Variations in Tropical Oceanic Cumulus Convection during TOGA COARE, Journal of the Atmospheric Sciences, 54, 639-655, 10.1175/1520-0469(1997)054<0639:dvitoc>2.0.co;2, 1997.

Tao, W. K., Chen, J. P., Li, Z. Q., Wang, C., and Zhang, C. D.: Impact of aerosols on convective clouds and precipitation, Reviews of Geophysics, 50, 10.1029/2011rg000369, 2012.

Twomey, S., and Warner, J.: Comparison of Measurements of Cloud Droplets and Cloud Nuclei, Journal of the Atmospheric Sciences, 24, 702-703, 10.1175/1520-0469(1967)024<0702:comocd>2.0.co;2, 1967.

Twomey, S.: Pollution and the planetary albedo, Atmospheric Environment (1967), 8, 1251-1256, https://doi.org/10.1016/0004-6981(74)90004-3, 1974.

Wang, Q., Li, Z., Guo, J., Zhao, C., and Cribb, M.: The climate impact of aerosols on the lightning flash rate: is it detectable from long-term measurements?, Atmospheric Chemistry and Physics, 18, 12797-12816, 10.5194/acp-18-12797-2018, 2018.

Wang, Y., Khalizov, A., Levy, M., and Zhang, R.: New Directions: Light absorbing aerosols and their atmospheric impacts, Atmospheric Environment, 81, 713-715, 10.1016/j.atmosenv.2013.09.034, 2013.

Welch, R. M., Sengupta, S. K., and Chen, D. W.: Cloud field classification based upon high spatial resolution textural features: 1. Gray level co-occurrence matrix approach, Journal of Geophysical Research: Atmospheres, 93, 12663-12681, 10.1029/JD093iD10p12663, 1988a.

Welch, R. M., Sengupta, S. K., and Kuo, K. S.: Marine Stratocumulus Cloud Fields off the Coast of Southern California Observed Using LANDSAT Imagery. Part II: Textural Analysis, Journal of Applied Meteorology, 27, 363-378, 10.1175/1520-0450(1988)027<0363:mscfot>2.0.co;2, 1988b.

Wielicki, B. A., and Welch, R. M.: Cumulus Cloud Properties Derived Using LANDSAT Satellite Data, Journal of Climate and Applied Meteorology, 25, 261-276, 10.1175/1520-0450(1986)025<0261:ccpdul>2.0.co;2, 1986.

Williams, M., and Houze Jr., R. A.: Satellite-Observed Characteristics of Winter Monsoon Cloud Clusters, Monthly Weather Review, 115, 505-519, 10.1175/1520-0493(1987)115<0505:socowm>2.0.co;2, 1987.

Wilson, A. M., Parmentier, B., and Jetz, W.: Systematic land cover bias in Collection 5 MODIS cloud mask and derived products — A global overview, Remote Sensing of Environment, 141, 149-154, https://doi.org/10.1016/j.rse.2013.10.025, 2014.

Xiao, H., Yin, Y., Jin, L., Chen, Q., and Chen, J.: Simulation of the effects of aerosol on mixed-phase orographic clouds using the WRF model with a detailed bin microphysics scheme, Journal of Geophysical Research: Atmospheres, 120, 8345-8358, 10.1002/2014jd022988, 2015.

Yang, X., Zhao, C., Guo, J., and Wang, Y.: Intensification of aerosol pollution associated with its feedback with surface solar radiation and winds in Beijing, Journal of Geophysical Research-Atmospheres, 121, 4093-4099, 10.1002/2015jd024645, 2016a.

Yang, X., Zhao, C., Zhou, L., Wang, Y., and Liu, X.: Distinct impact of different types of aerosols on surface solar radiation in China, Journal of Geophysical Research-Atmospheres, 121, 6459-6471, 10.1002/2016jd024938, 2016b.

Yang, X., Zhao, C., Zhou, L., Li, Z., Cribb, M., and Yang, S.: Wintertime cooling and a potential connection with transported aerosols in Hong Kong during recent decades, Atmospheric Research, 211, 52-61, 10.1016/j.atmosres.2018.04.029, 2018.

Yang, Y., Fan, J., Leung, L. R., Zhao, C., Li, Z., and Rosenfeld, D.: Mechanisms Contributing to Suppressed Precipitation in Mt. Hua of Central China. Part I: Mountain Valley Circulation, Journal of the Atmospheric Sciences, 73, 1351-1366, 10.1175/jas-d-15-0233.1, 2016c.

Yang, Y., Zhao, C., Dong, X., Fan, G., Zhou, Y., Wang, Y., Zhao, L., Lv, F., and Yan, F.: Toward understanding the process-level impacts of aerosols on microphysical properties of shallow cumulus

https://doi.org/10.5194/acp-2020-845
Preprint. Discussion started: 13 October 2020

cloud using aircraft observations, Atmospheric Research, 221, 27-33, 10.1016/j.atmosres.2019.01.027, 2019.

Zhao, C., Klein, S. A., Xie, S., Liu, X., Boyle, J. S., and Zhang, Y.: Aerosol first indirect effects on non-precipitating low-level liquid cloud properties as simulated by CAM5 at ARM sites, 39, 10.1029/2012gl051213, 2012.

Zhao, C., and Garrett, T. J.: Effects of Arctic haze on surface cloud radiative forcing, Geophysical Research Letters, 42, 557-564, 10.1002/2014gl062015, 2015.

Zhao, C., Lin, Y., Wu, F., Wang, Y., Li, Z., Rosenfeld, D., and Wang, Y.: Enlarging Rainfall Area of Tropical Cyclones by Atmospheric Aerosols, Geophysical Research Letters, 45, 8604-8611, 10.1029/2018gl079427, 2018a.

Zhao, C., Qiu, Y., Dong, X., Wang, Z., Peng, Y., Li, B., Wu, Z., and Wang, Y.: Negative Aerosol-Cloud re Relationship From Aircraft Observations Over Hebei, China, Earth and Space Science, 5, 19-29, 10.1002/2017ea000346, 2018b.

Zhao, C., Zhao, L., and Dong, X.: A Case Study of Stratus Cloud Properties Using In Situ Aircraft Observations over Huanghua, China, 10, 19, 2019.

Zhao, C., Yang, Y., Fan, H., Huang, J., Fu, Y., Zhang, X., Kang, S., Cong, Z., Letu, H., and Menenti, M.: Aerosol characteristics and impacts on weather and climate over the Tibetan Plateau, National Science Review, 7, 492-495, 10.1093/nsr/nwz184, 2020.

Zhou, S., Yang, J., Wang, W. C., Zhao, C., Gong, D., and Shi, P.: An observational study of the effects of aerosols on diurnal variation of heavy rainfall and associated clouds over Beijing–Tianjin–Hebei, Atmos. Chem. Phys., 20, 5211-5229, 10.5194/acp-20-5211-2020, 2020.

Zhou, T., Yu, R., Chen, H., Dai, A., and Pan, Y.: Summer Precipitation Frequency, Intensity, and Diurnal Cycle over China: A Comparison of Satellite Data with Rain Gauge Observations, Journal of Climate, 21, 3997-4010, 10.1175/2008jcli2028.1, 2008.

https://doi.org/10.5194/acp-2020-845
Preprint. Discussion started: 13 October 2020

Atmospheric Chemistry and Physics
Open Access
EGU
Discussions

Figures

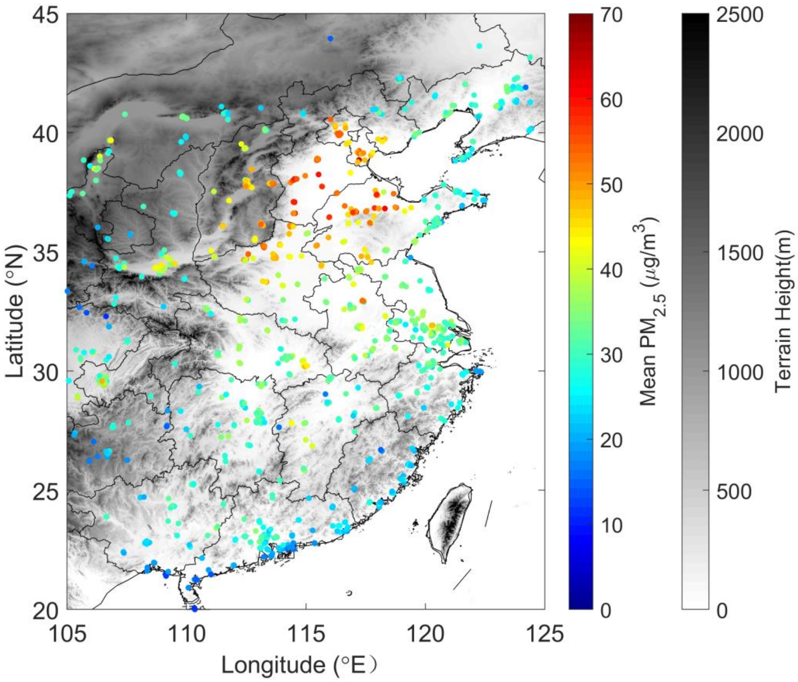

Figure 1. Surface elevation and the mean value of ground-based $PM_{2.5}$ measurements over eastern China. The terrain height (TH) of this region is represented with gray shading. Colored dots show the mean $PM_{2.5}$ concentration from 1205 surface stations during May-September in 2016-2017 over this area.

https://doi.org/10.5194/acp-2020-845
Preprint. Discussion started: 13 October 2020

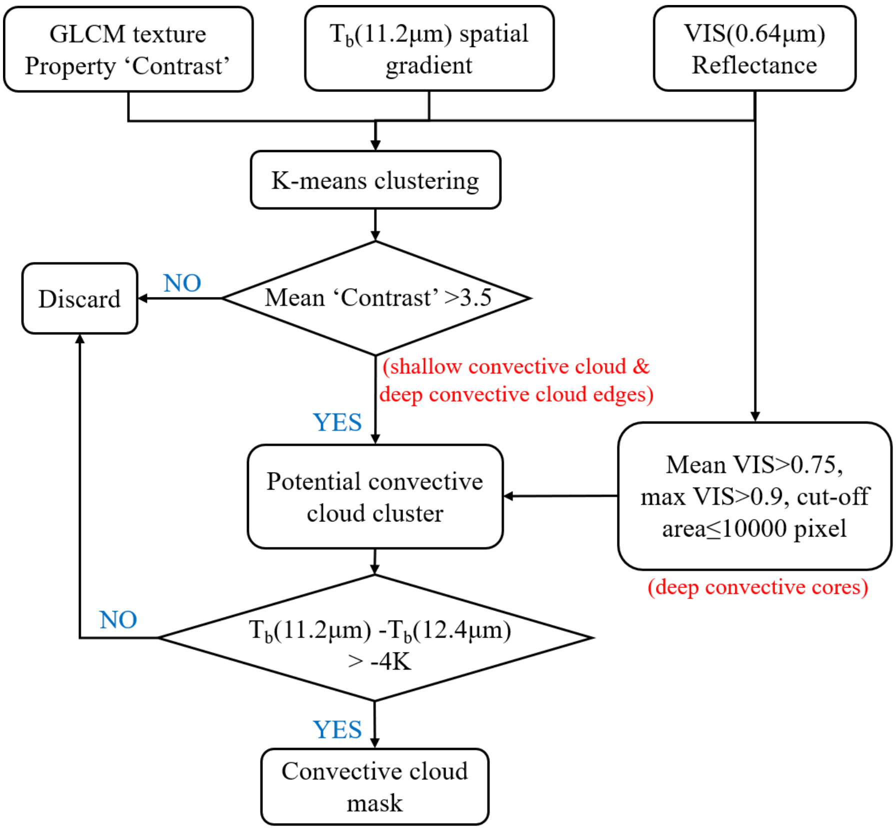

1018

1019 **Figure 2**. Flowchart of the convective cloud identification method.

1020

https://doi.org/10.5194/acp-2020-845
Preprint. Discussion started: 13 October 2020

Atmospheric Chemistry and Physics Discussions

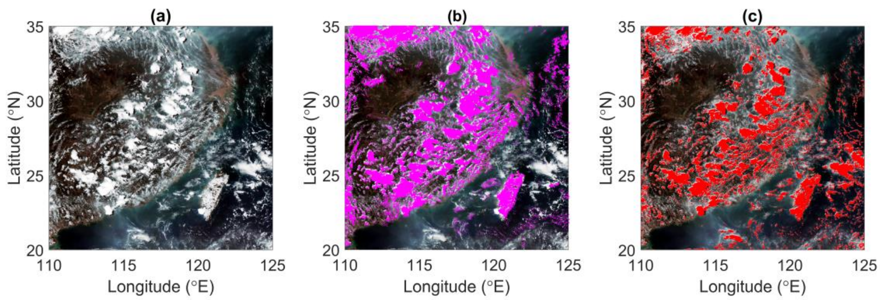

Figure 3. Comparison between MODIS cloud mask and the cloud identified by our convective cloud (CC) mask, at 13:40 LT on July 30th, 2016. (a) The true color image, (b) MODIS cloud mask data from the MYD35 product (magenta points), and (c) convective clouds (CC) identified using the TCT-CID method.

https://doi.org/10.5194/acp-2020-845
Preprint. Discussion started: 13 October 2020

Atmospheric Chemistry and Physics
Discussions
Open Access

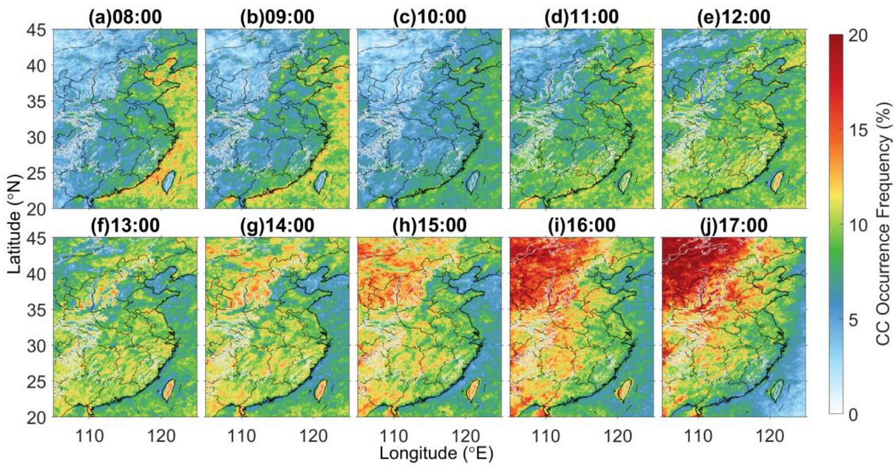

Figure 4. Diurnal cycle of convective cloud (CC) occurrence frequency (OF) during daytime. The gray contour lines in each figure represent the terrain height (TH) at 1000 m. Most locations west of the contour line have TH >1000 m, whereas terrain east of the contour lines has TH <1000 m.

https://doi.org/10.5194/acp-2020-845
Preprint. Discussion started: 13 October 2020

Atmospheric Chemistry and Physics
Open Access
Discussions

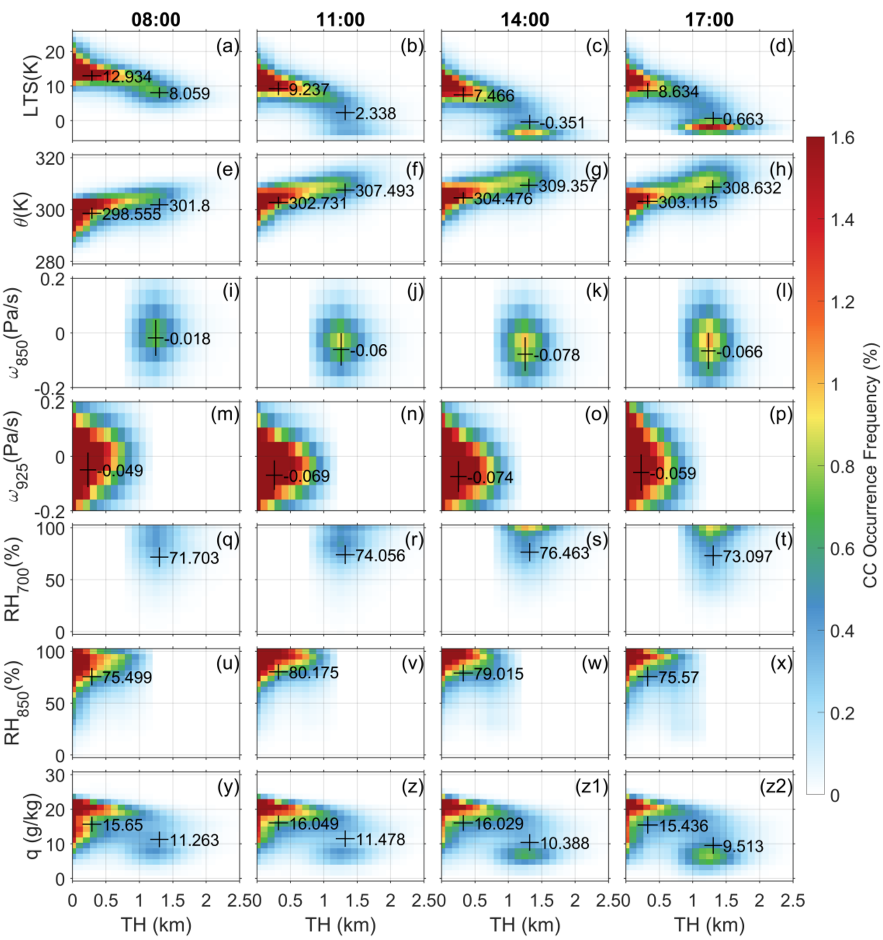

Figure 5. Over-land convective cloud (CC) occurrence frequency (OF) with respect to terrain height (TH) and (a-d) lower-tropospheric stability (LTS), (e-h) potential temperature (θ), (i-l) vertical pressure velocity at 850 hPa (ω_{850}) over terrain above 1000 m, (m-p) vertical pressure velocity at 925 hPa (ω_{925}) over terrain below 1000 m, (q-t) relative humidity at 700 hPa (RH_{700}) over terrain above 1000 m, (u-x) relative humidity at 850 hPa (RH_{850}) over terrain below 1000 m, (y-z2) specific humidity at surface (q). The columns represent local time over the ROI of 08:00, 11:00, 14:00 and 17:00, respectively. Black crosses and numbers beside mark the mean values of the variables over regions with terrain height below 1000 m and above 1000 m, crosses mark the

https://doi.org/10.5194/acp-2020-845
Preprint. Discussion started: 13 October 2020

Atmospheric Chemistry and Physics Discussions

standard deviations of the variables.

Atmospheric Chemistry and Physics
Discussions

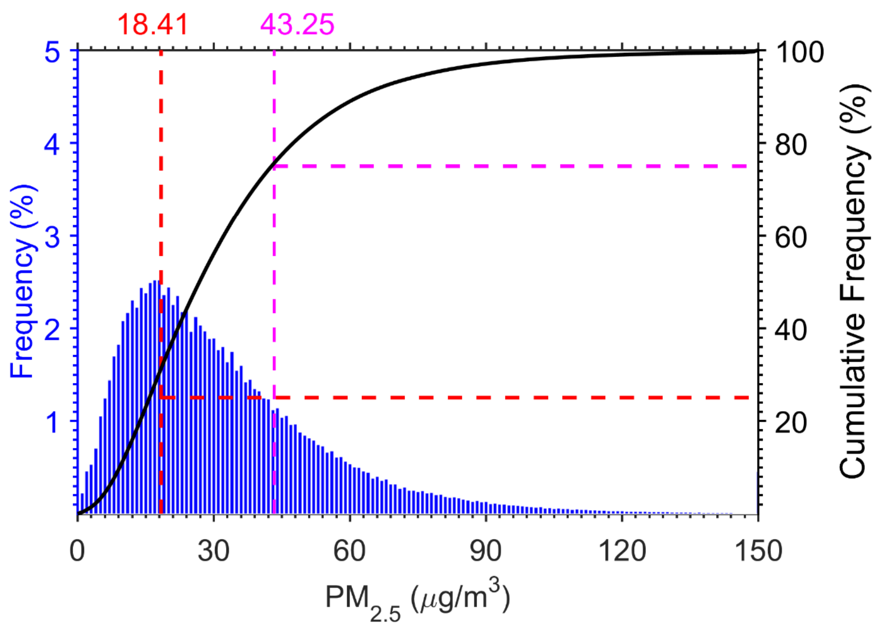

Figure 6. Mean $PM_{2.5}$ concentration distribution for 1205 sites over Eastern China during daytime (08:00-17:00 local time). Blue bars and the black line show the frequency and cumulative frequency of mean $PM_{2.5}$, respectively. The mean value of the top quarter is marked by the magenta dashed line, and the mean value of the bottom quarter is marked with the red dashed line.

https://doi.org/10.5194/acp-2020-845
Preprint. Discussion started: 13 October 2020

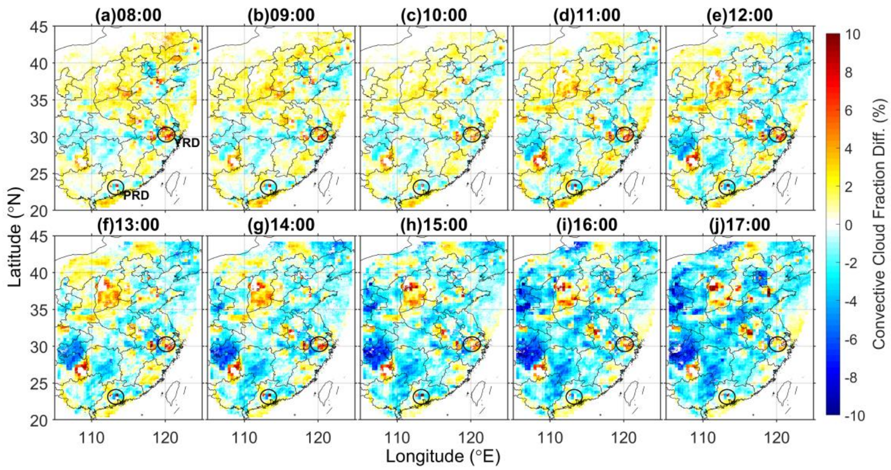

Figure 7. Diurnal changes of convective cloud fraction (CCF) difference between polluted and clean conditions (Polluted-Clean) during May-September in 2016-2017. Time marked above each figure is the local time. Black circles mark the Yangtze River Delta (YRD) and Pearl River Delta (PRD). (Note that grid points are plotted only if they exceed the 95% significance level ($p < 0.05$) according to the Pearson's χ^2 test).

https://doi.org/10.5194/acp-2020-845
Preprint. Discussion started: 13 October 2020

Atmospheric Chemistry and Physics Discussions

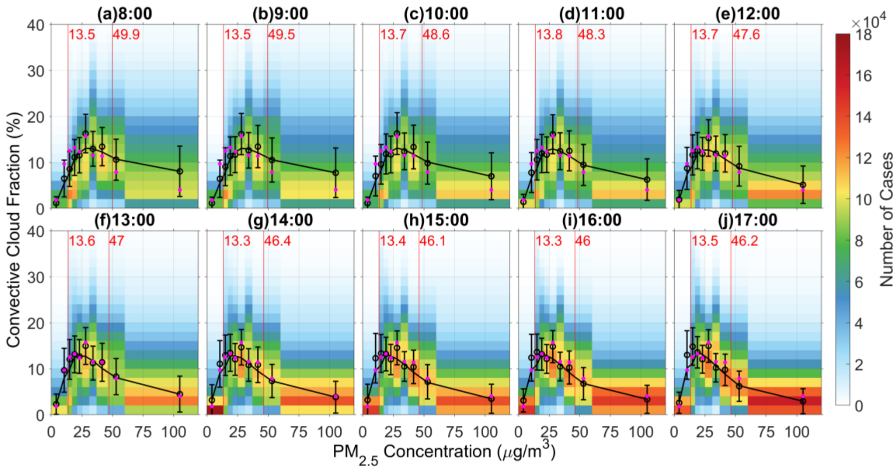

Figure 8. Convective cloud fraction with respect to $PM_{2.5}$ concentration at different times of day during May-September, 2016-2017. Color shading indicates the number of cases corresponding to each specific convective cloud fraction (CCF) and $PM_{2.5}$ bin. Note that $PM_{2.5}$ is separated into ten equal-sample bins. Black circles and error bars are the mean values and standard deviations of CCF in each $PM_{2.5}$ bin within each hour, magenta dots indicate the mean CCF over all times. Black solid lines represent the three-point moving average of the black circles. Red solid lines (with red numbers) mark the mean polluted and clean thresholds during each hour.

https://doi.org/10.5194/acp-2020-845
Preprint. Discussion started: 13 October 2020

Atmospheric Chemistry and Physics
Discussions

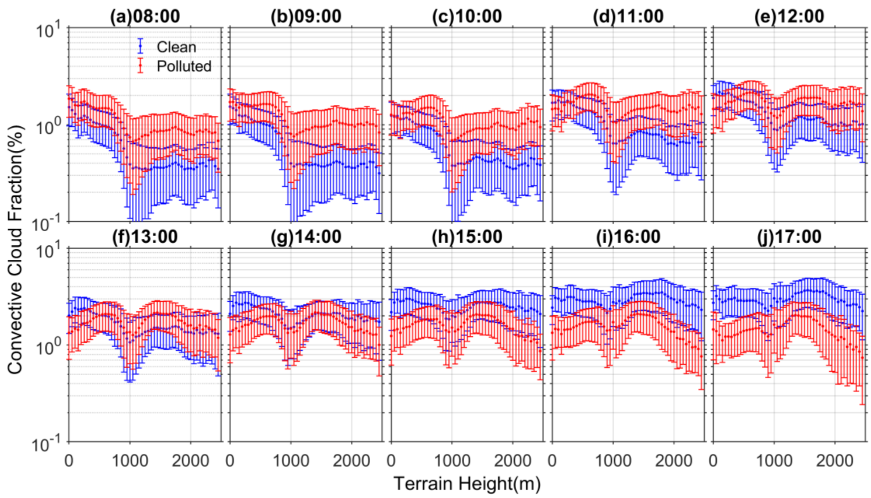

Figure 9. Convective cloud fraction (CCF) normalized by the total number of cases with respect to terrain height changes during May-September, 2016-2017. Data for polluted conditions are plotted in red, whereas those for clean conditions are shown in blue. Dots and error bars are the mean values and standard deviations of the fractions in each TH bin.

https://doi.org/10.5194/acp-2020-845
Preprint. Discussion started: 13 October 2020

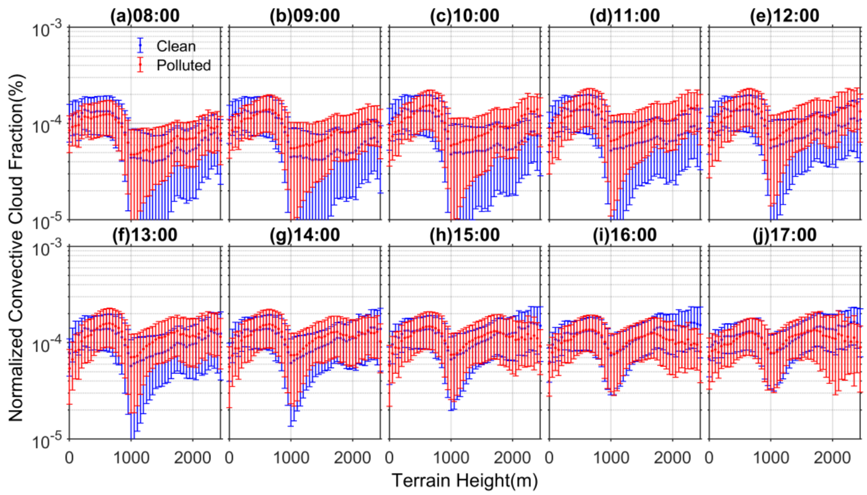

1076

1077 **Figure 10**. Same as Figure 9, but for CCF that is normalized by the number of cases
1078 under polluted and clean conditions during each hour, respectively (Equation 8).

1079

https://doi.org/10.5194/acp-2020-845
Preprint. Discussion started: 13 October 2020

Atmospheric Chemistry and Physics
Discussions

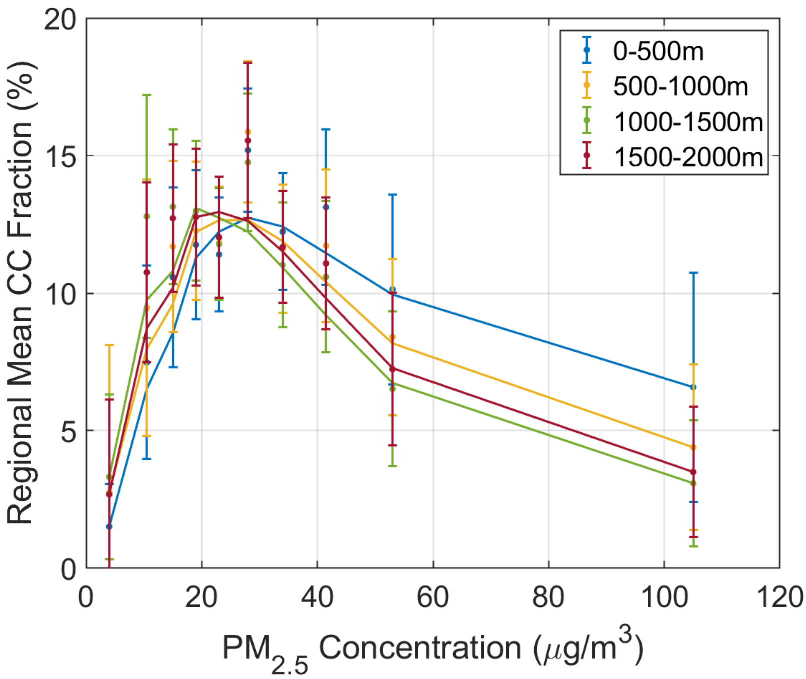

Figure 11 Convective cloud fraction (CCF) over regions with terrain heights in the range 0-500 m (blue), 500-1000 m (yellow), 1000-1500 m (green) and 1500-2000 m (red) with respect to $PM_{2.5}$ concentration during May-September, 2016-2017. Ten equally sampled $PM_{2.5}$ bins are defined for each terrain height range. The standard deviations are shown as error bars. Each solid line represents the three-point moving average for dots in the corresponding color.

https://doi.org/10.5194/acp-2020-845
Preprint. Discussion started: 13 October 2020

Atmospheric Chemistry and Physics
Discussions
Open Access
EGU

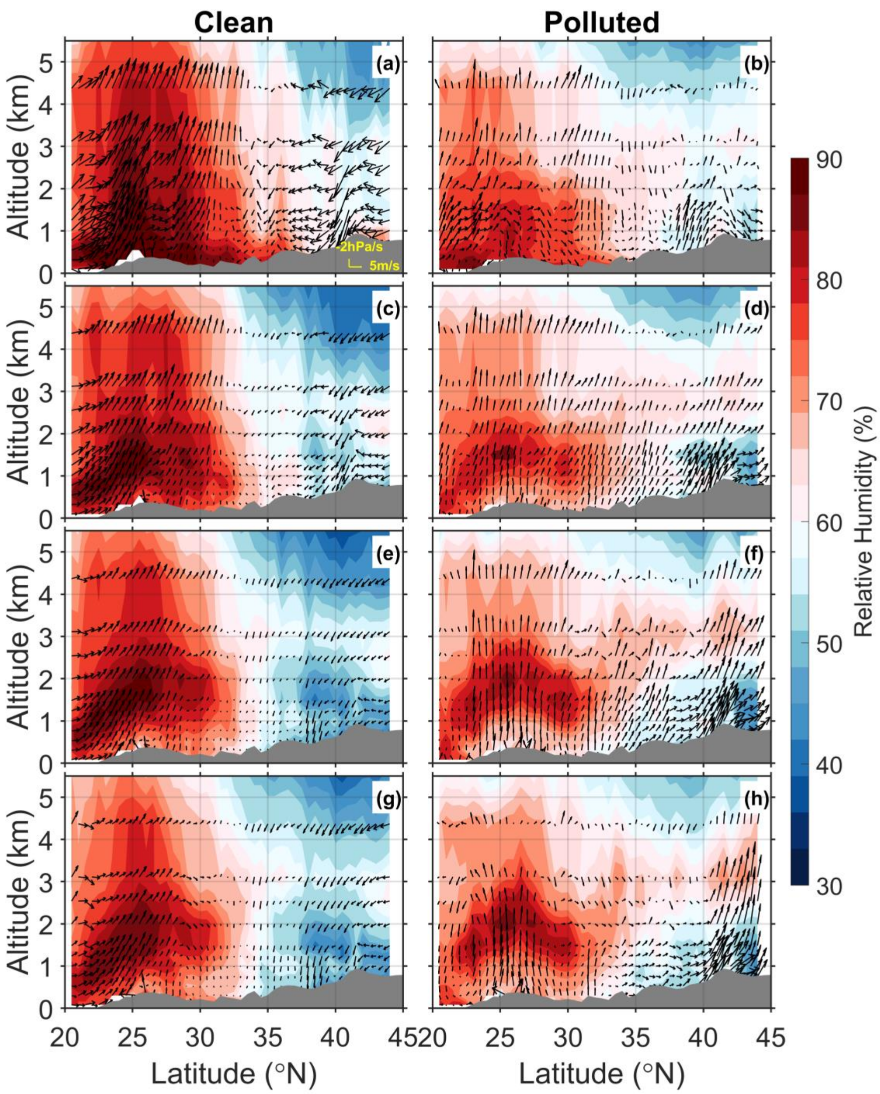

Figure 12. Latitude-altitude cross-sections of mean relative humidity (color-shaded) and mean meridional-vertical wind (vectors) over the continent, averaged along 105 to 125°E for clean (left panel) and polluted (right panel) conditions at (a, b) 08:00 LT, (c, d) 11:00 LT, (e, f) 14:00 LT and (g, h) 17:00 LT during May-September from 2016 to

https://doi.org/10.5194/acp-2020-845
Preprint. Discussion started: 13 October 2020

2017. Vectors are constructed from the easterly wind (u) and vertical velocity (ω), scaled with -100. Gray shaded parts are the meridional mean terrain heights within ROI.

https://doi.org/10.5194/acp-2020-845
Preprint. Discussion started: 13 October 2020

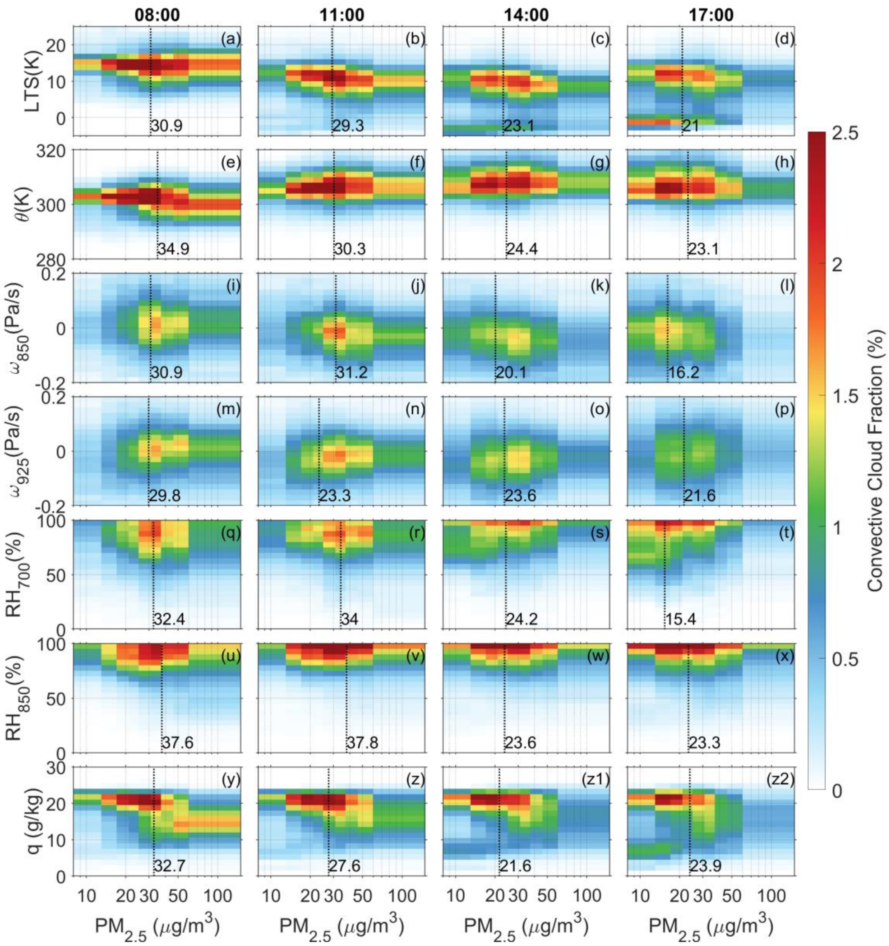

Figure 13. The joint distribution of convective cloud fraction (CCF) with respect to $PM_{2.5}$ concentration and (a-d) lower-tropospheric stability (LTS), (e-h) potential temperature (θ), (i-l) vertical pressure velocity at 850 hPa (ω_{850}) over terrain above 1000 m, (m-p) vertical pressure velocity at 925 hPa (ω_{925}) over terrain below 1000 m, (q-t), relative humidity at 700 hPa (RH_{700}) over terrain above 1000 m, (u-x) relative humidity at 850 hPa (RH_{850}) over terrain below 1000 m, (y-z2) relative humidity at the surface ($RH_{surface}$). Each column represents a different local time during the day within the ROI, specifically at 08:00, 11:00, 14:00 and 17:00. Black dashed lines and the numbers

https://doi.org/10.5194/acp-2020-845
Preprint. Discussion started: 13 October 2020

Atmospheric Chemistry and Physics Discussions

beside mark the mean tipping points of CCF at different thermodynamic, dynamical and humidity levels. Note that x-axis is in log scale.

https://doi.org/10.5194/acp-2020-845
Preprint. Discussion started: 13 October 2020

1108 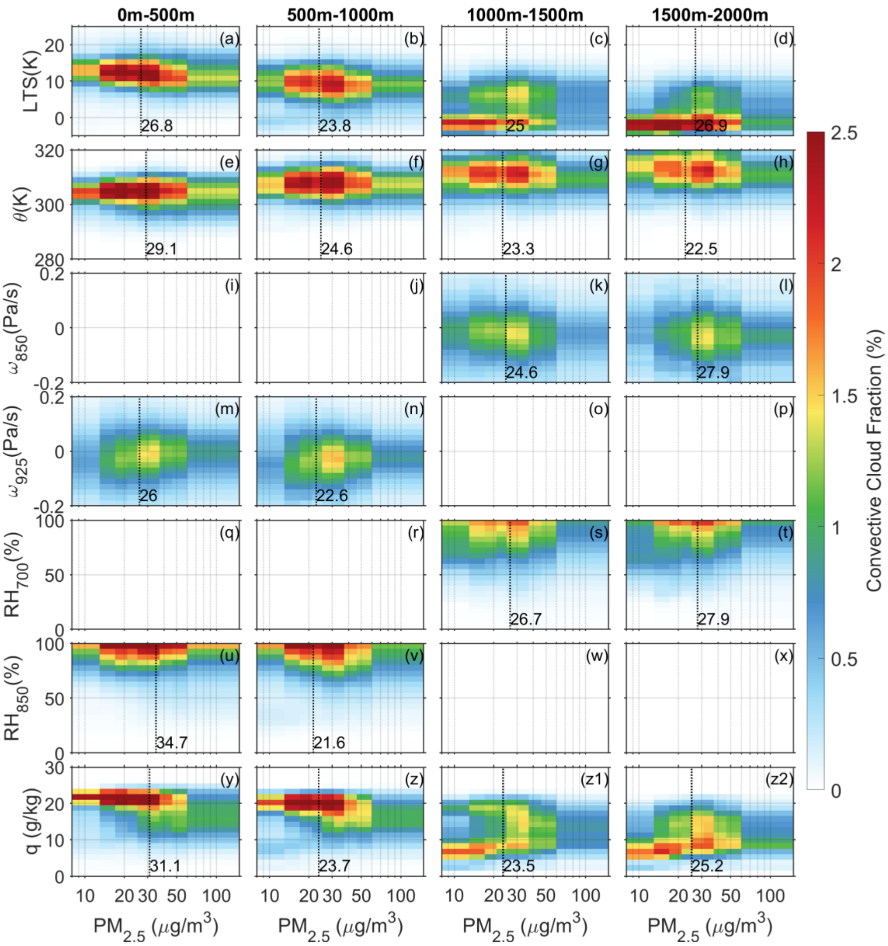

1109 **Figure 14**. Same as Figure 13, but for different terrain heights; each column represents

1110 a different terrain height range.

1111